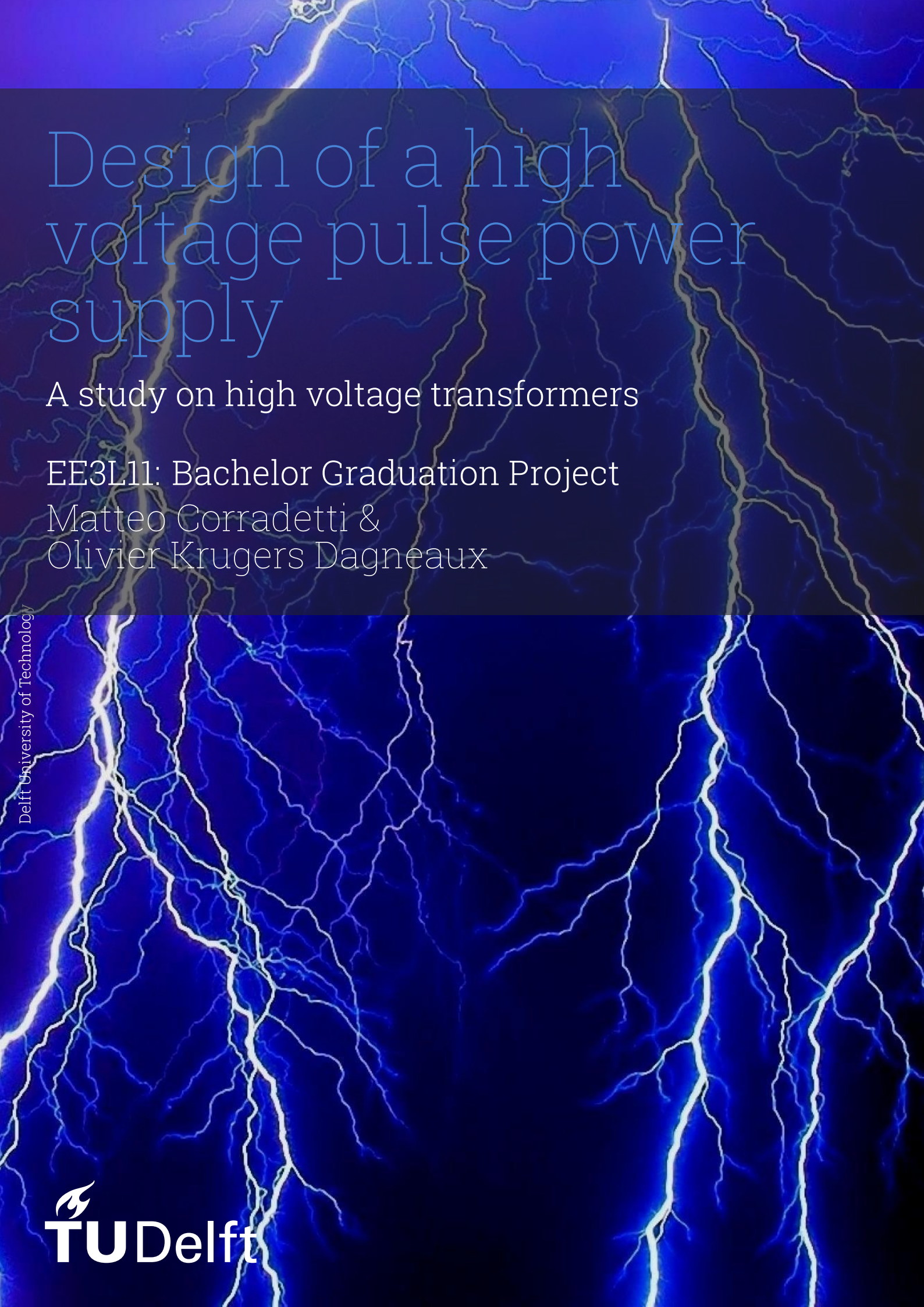

Design of a high voltage pulse power supply

A study on high voltage transformers

EE3L11: Bachelor Graduation Project

Matteo Corradetti &
Olivier Krugers Dagneaux

Delft University of Technology

TU Delft

Design of a high voltage pulse power supply

A study on high voltage transformers

by

Matteo Corradetti &
Olivier Krugers Dagneaux

Supervisors:	Prof. dr. ir. J. van Turnhout
	dr. ir. H.W. van Zeijl
	dr. ir. M. Ghaffarian Niasar
	dr. L. Wymenga
Project Duration:	April, 2025 - June, 2025
Faculty:	EEMCS, Delft

TU Delft

Abstract

This report covers the design of a high voltage power supply that is designed for seed disinfection applications using plasma-activated water (PAW). The goal is to have a safe and reliable pulse power supply that can be used to power a Dielectric Barrier Discharge (DBD) load.
Multiple setups were designed and analyzed. Different transformers were designed and compared with differing core dimensions, inner radius, number of windings and type of winding. Furthermore, a bipolar driver was built and tested.

The results demonstrate that the current design is a solid foundation for small-scale plasma-activated water generation and that it can be scaled with a segmented setup consisting of multiple smaller loads. Future iterations should focus on improving thermal dissipation, switching efficiency, and transformer insulation.

Preface

This thesis is written for the Bachelor Graduation Project of the BSc Electrical Engineering at TU Delft. The project was sponsored by Bejo Seeds, an international seed supplier with its headquarters located in the Netherlands. Currently, Bejo Seeds uses warm water baths for seed disinfection. However, Bejo is investigating alternative methods which are more sustainable and effective. This is where plasma-activated water comes into the picture. The goal of the complete project was to make a prototype that can generate plasma-activated water. Additionally, its potential to disinfect seeds was also investigated.

We express our gratitude to our supervisors M. Ghaffarian Niasar, J. van Turnhout, H. van Zeijl and L. Wymenga for their guidance during the project. We thank Yvette Bakker of Bejo Seeds for the office tour at Bejo Seeds headquarters. Finally, we thank our colleagues, T. Mertens, B. van de Ruit, A. Sachar and T. Neef for the collaboration.

Matteo Corradetti &
Olivier Krugers Dagneaux
Delft, July 2025

Contents

1 Introduction

1.1. Seed disinfection

Food security has become a bigger concern over the past years. Due to the growing risk of geographical pathogen spread, greater emphasis must be placed on seed sterilization [1]. Additionally, as the agricultural land remains limited, a higher yield per area is necessary to keep up with the increasing global food demand. One way to increase yield is to ensure a higher germination rate of seeds into healthy plants. For this, efficient seed disinfection is essential. Seeds infected with fungi or bacteria have a lower germination rate. By disinfecting these seeds before planting them, the yield increases [2]. Currently, warm water baths are used to disinfect seeds. On top of lowering the germination rate, heating these baths up consumes a large amount of energy. Moreover, the water must be regularly changed which leads to a high water consumption. Therefore, a more sustainable solution is needed while keeping the disinfection rate of the seeds high.

Cold Atmospheric Plasma (CAP) might be a sustainable and effective solution for the disinfection of seeds. CAP is a type of plasma which is produced by applying strong electric fields on a gas. Contrary to thermal plasma which is made by heating a gas to extremely high temperatures, CAP does not reach temperatures that could damage seeds. Reactive oxygen and nitrogen molecules are formed in this process to make CAP. These species disinfect the seeds by eliminating pathogens that are localized on the surface of the seeds [3]. One of the applications of cold atmospheric plasma is plasma-activated water (PAW).

1.2. State of the art

A promising new application of plasma is plasma-activated water. PAW is water that is exposed to a plasma. This can be done in various ways. One example is plasma-activated aerosol (PAA), where cold atmospheric plasma is formed directly within the aerosol. This is also known as plasma-activated aerosol. Another example is where air, exposed to cold atmospheric plasma is pumped into water. A part of the reactive oxygen and nitrogen molecules that are formed in the plasma state diffuse into the water. Thus, the plasma-activated water has similar disinfecting properties to cold atmospheric plasma.

1.3. Group division

This project is divided into multiple sub projects. The three sub groups of the project are the following

- Sensing and measuring
- Plasma generating
- High voltage power supply

This report covers the design and the corresponding research of the high voltage power supply. A visual division of the complete project is given in figure 1.1.

The high voltage power supply group is responsible for a reliable power supply which can generate high voltage pulses. A detailed list of the requirements are given in section 2.

The plasma generating group is responsible for efficiently creating cold atmospheric plasma.

The sensing group is responsible for making PAW through a Venturi tube, disinfecting the seeds and measuring the quality of the PAW. A Venturi tube is a device that can be used to inject a gas into a liquid though the Venturi effect.

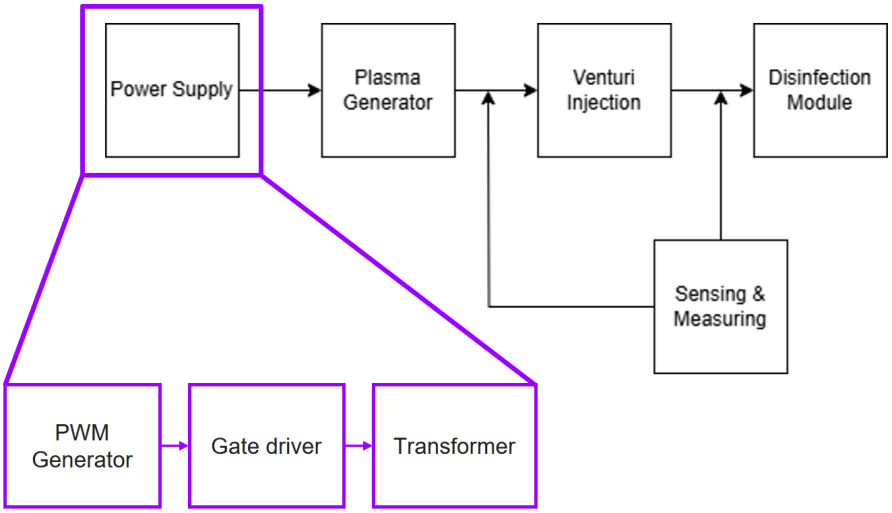

Figure 1.1: Project overview

1.4. Document structure

This report follows the different design process of the high voltage power supply. In chapter 2 the requirements of the power supply are given. Followed by chapters 3 and 4 where the design of the driver and the transformer are justified. In chapter 5 the results of the driver and transformer are given. Finally in chapter 6, the results are compared with the requirements and future improvements are suggested and in chapter 7 the conclusion is given.

2

Program of Requirements

In the following chapter the program of requirements for the high voltage power supply is given and discussed. The requirements are categorized into either functional requirements or technical requirements. Functional requirements describe the system's features and user interactions. The technical requirements however, describe how the system should perform including constraints, quality standards and specifications.

Since the project is requested by Bejo Zaden, the requirements have been custom-defined with Bejo Zaden to align with their operational needs, technical constraints, and project objectives. A requirement matrix was made to compare the different solutions and identify the most suitable one.

Functional requirements

- Power supply must be frequency adjustable (10kHz-100kHz)
- Power supply must be duty cycle adjustable (20%-80%)
- Power supply should be voltage adjustable (0-10kV)
- Power supply should have a consistent output
- Power supply should be reliable
- Power supply could have a long lifespan
- Power supply could be scalable
- Power supply would be serviceable

Technical requirements

- Power supply must sustain short arcing events
- Power supply should drive capacitive loads in the pico farad range
- Power supply should produce square pulse waves
- Power supply should have low distortion/error when capacitive load in pF range is connected
- Power supply should have a simple driving circuit
- Power supply could have low thermal dissipation (actively cooled)

[4]

2.1. DC vs. AC

Research has been done to identify whether direct current or alternating current has a better effect on the plasma generating. In theory, both DC and AC can generate plasma. According to Kurt [5]: "DC driven plasmas are faster and more efficient, with greater utility, than AC driven plasmas." However, AC dielectric barrier discharge can operate at atmospheric pressure, while DC driven discharges required

sub-atmospheric pressures (10–760 Torr) in their setup to avoid arcing and as a consequence excessive heating. It is possible to have controllable DC driven dielectric barrier discharge with atmospheric pressure but a complex circuit is necessary that limits the current. Hence, the decision was made to make an AC power supply.

The next questions that arise are what frequency range and what waveforms are optimal for the dielectric barrier discharge production. Wei (2022) [6] states that ozone production is highly frequency dependent. The optimal frequency range is the kHz range. Moreover, Wei compares the ozone production for sinusoidal waveforms and pulse waveforms. Pulse waveforms lead to a higher ozone production than sinusoidal waveform. On the other hand, the circuitry to supply high voltage sinusoidal waveforms is easier and overall more efficient than pulse waveforms. Finally, according to Paschen's law [7] and in communication with the other subgroups, it was agreed that the power supply will be able to supply a maximum voltage level of around 10 kV.

Table 2.1: Requirement matrix

	Performance	Reliability	Cost
Mazilli ZVS driver + transformer			
High voltage switching (cascode)			
Unipolar pulse switching + transformer			
Bipolar pulse switching + transformer			

3

Driver Circuit

A high voltage power supply is composed of three main components as shown in figure 1.1. This chapter elaborates on the Pulse Width Modulation (PWM) generator and switching circuitry. The primary coil of the transformer will be connected to the output of the final driver circuit. During this project, multiple commercial driver circuits were tested and two driver circuit were designed. Both of the circuits were designed to output a square wave pulse. The Unipolar driver circuit was designed to be a simple and cheap circuit that generates a single polarity pulse. The Bipolar driver on the other hand was a more complex circuit which can make bipolar square pulses.

3.1. PWM Generator

To drive the circuit, a square pulse generator was required. This generator had to be frequency and duty cycle adjustable. To generate this signal two options have been considered. The first option was a small circuit based on a timer Integrated Circuit (IC) like the NE555P. This was the cheaper option but lacks features such as complementary PWM signals which are needed for the bipolar driver. The second option, that was pursued, was a micro controller based PWM generator. The micro controller that was initially used was based on the ESP32-C3 platform. This controller is designed for low power applications, leading to the removal of the Motor Control Pulse Width Modulation (MCPWM) peripheral. The ESP32-C3 can be used to generate a single PWM signal but it does not incorporate a synchronization feature which is necessary to generate a complementary signal. Moreover, it is not possible to program a dead time between the pulses, which is necessary for the bipolar driver. A dead time is a certain period between each cycle where all signal outputs are zero. This is necessary to prevent the two complementary series connected switches from being closed at the same time.

Later, a ESP32-S3 development board was used which, in combination with the MCPWM.h library, was able to generate two complementary signals as seen figure B.1 . To ensure safe frequency and duty cycle adjustments, the integrated WiFi module of the development board was used. This enabled the operator to connect to the PWM generator on their phone or computer from a safe distance. A screenshot of the PWM web server can be seen in figure B.2

3.2. Commercially Available Circuits

As part of this project, a commercially purchased ozone generator was bought which is shown in figure B.14. This ozone generator consisted of a coaxial tube electrode and a high voltage AC power supply that is powered by the mains voltage. The Ozone generator advertises an ozone production of 10g per hour. During testing, both the tube and driver reached a high temperature of around $80\,^{\circ}\mathrm{C}$. After the dissection, it was noted that the glass tube used as the insulator was broken, likely causing the electrodes to arc. These thermal arcs may have posed a high load on the driver, leading to an increase in temperature. Upon further inspection, the circuit was found to be poorly designed with a low cost being its primary requirement. The schematic of the circuit can be seen in figure 3.1. During the conduction of a test without a load the circuit broke down. Thus, no further measurements could be taken

with this circuit. This event further emphasized the unreliability of the circuit. The circuit's transformer was casted in a fire retardant resin and the circuit was covered in a thin layer of resin. The irreparability and inefficient design of the power supply makes it inconvenient and unusable for larger scale or commercial applications. A circuit diagram has been made of the thyristor based power supply.

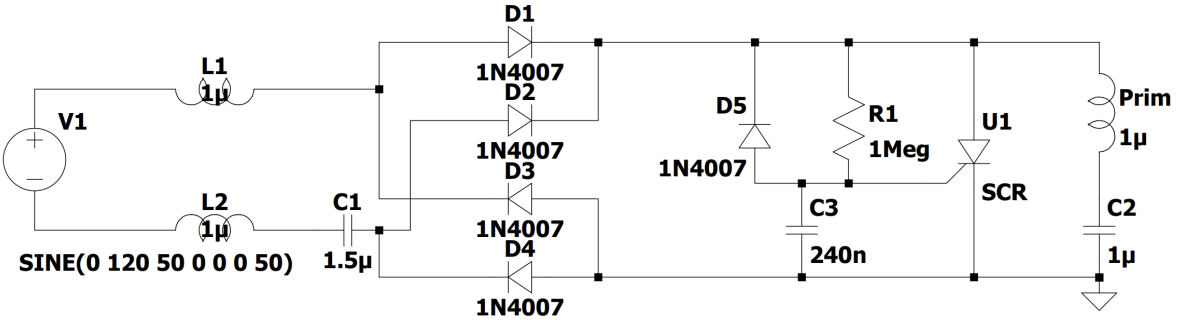

Figure 3.1: Schematic of cheap commercial thyristor based Circuit

The circuit takes in mains voltage which is passed through a common mode choke. This component acts as a filter to prevent high frequency noise from entering the circuit [8]. The component consists of two inductors turned in the same direction around a single ferrite core. Common mode noise which may enter the circuit from mains and exit from parasitic capacitance will pass through this component in the same direction from both input terminals.

When common mode noise passes though the inductors, the magnetic flux will add up in the core, as shown by the arrows in figure 3.2. This makes the component act like a large inductor. This large inductor imposes a large impedance to high frequency common mode noise. Differential signal currents, which are desired, will lead to the cancellation of the flux inside of the core and will therefore perceive the component as a small inductor

[9].

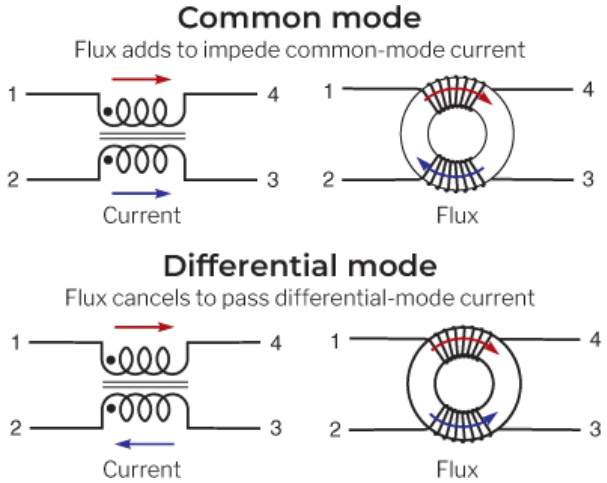

Figure 3.2: Visual representation of magnetic flux in a common mode choke [10]

Due to the resin layer, the thyristor model could be retrieved from the circuit. A thyristor, also called a Silicon-Controlled Rectifier (SCR), is a four layered semiconductor device which is often used as a switch in high power applications [11]. The point at which a thyristor starts conducting is determined by the applied gate voltage. The circuit utilizes the phase angle firing method. This means that the diode conducts at a specific phase angle during each cycle as seen in figure 3.3 [12]. The circuit utilizes a

full bridge rectifier, doubling the switching frequency from 50Hz to 100Hz. When it is in the conduction mode, the thyristor pulls down the voltage on the LC-circuit creating a pulse on the output. This method is simple and cheap, but wastes a lot of energy during the SCR conduction mode.

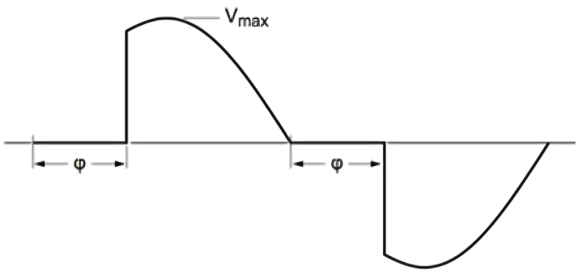

Figure 3.3: Phase angle switching thyristor [13]

3.2.1. Cheap H-bridge modules

Two compact full bridge circuits have been purchased which are shown in figure 3.4. The BTS7960 module contains half bridge ICs which together form a full bridge, also called H-bridge due to its shape. The L298N board uses a single IC which contain two H-bridges. The two modules are often used for DC motor driving applications but may also be used for low power transformer switching. The L298N based circuit is too weak to handle any significant load. The BTS7960 on the other hand is rated for a continuous current of 10A, but this is likely not sustainable for long periods of time due to overheating issues. Further specifications are given in table 3.1. The main limitation of the BTS7960 for this application is the relatively low operating frequency of 25kHz which does not meet the project requirements.

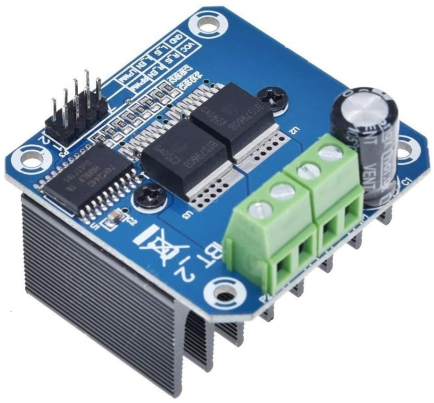

(a) BTS7960 H-bridge module [14]

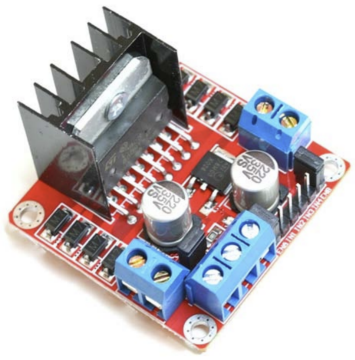

(b) L298N H-bridge module [15]

Figure 3.4: compact full bridge circuits

Table 3.1: Comparison of BTS7960 and L298N Motor Driver Modules

Specification	BTS7960	L298N
Driver Type	Half-Bridge (2x)	Dual H-Bridge
Input Voltage Range	5.5V - 28V	5V - 35V
Peak Current	43A	2A (per bridge)
Continuous Current	10A	1A (per bridge)
PWM Frequency	Up to 25kHz	Up to 40kHz
Logic Voltage	3.3V/5V	5V
Protection Features	OCP, OVP, TSD	Basic thermal shutdown
Cost	€5	€2

3.2.2. Mazzilli Zero Voltage Switching driver

The Mazzilli Zero Voltage Switching (ZVS) driver is a simple self oscillating circuit. The circuit diagram can be seen in figure 3.5. The driver is of the half bridge topology and operates at the resonant frequency of its LC-circuit which is often in the 20kHz range. The inductor in the tank circuit is the primary coil of the high voltage transformer. This means that the operating frequency depends on the driver load. The ZVS driver, like the name implies, is a type of soft switching that switches its MOSFETs when their drain to source voltage (V_{DS}) is equal to zero. By switching at the zero-crossing, it is possible to efficiently drive high power loads [16].

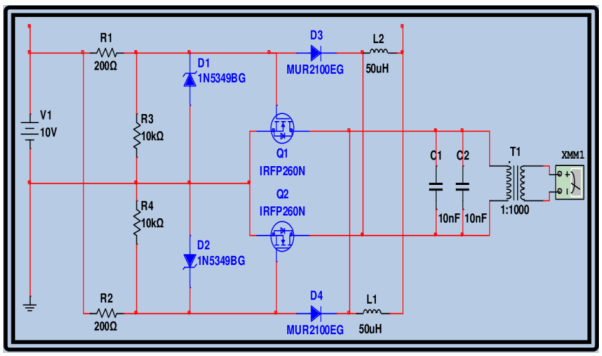

Figure 3.5: ZVS driver schematic [16]

As soon as power is supplied to the circuit, the MOSFET gates will start charging up. The gate driving circuit may seem symmetrical but in reality no component is equal. This means that one of the MOSFETs will reach its threshold first and will therefore start conducting before the other. During the conduction state the LC circuit is powered leading to oscillations. During the zero-crossing, a fast switching diode will discharge the gate of the conducting MOSFET. When discharging process occurs, the other switch then charges up and continues this cycle. The main advantage of this circuit is its simplicity. This benefit however is met with many limitations, the first one being that the operator has no control over the switching frequency. Additionally, the gate driving circuit is rather inefficient and slow. The 200Ω resistors R1 and R2 in figure 3.5 quickly heat up due to their low resistance. The inductors L1 and L2 face a similar problem as they are in series with the primary. These components require additional heat dissipation which are often not added from the factory. The maximum operating frequency may be increased with a gate driver and faster switching MOSFETs. Even though this can be done cheaply, it takes away from its main benefit being its simplicity.

3.3. Switch Choice

When designing the driver circuits, a choice to use technology for the power switches was made. After taking the switching speed and cost into consideration, it was opted to use Silicon MOSFETs. Gallium Nitride Field-Effect Transistors (GaN FETs) or Silicon Carbide (SiC) MOSFETs offer much higher switching speeds but may be three times as expensive. Given the limited frequency range (20kHz–100kHz), cost became a more significant factor in this decision.

The MOSFET that was predominantly used during this project is the IRFP460A N-channel MOSFET. This choice was primarily based on the relatively high power requirements of the driver. The driver must be designed to withstand a high transient load, ensuring its integrity during possible arcing events. This level of robustness may be lowered when operating under more stable and arcing safe conditions.

3.4. Unipolar Driver

The unipolar driver is based on a single N-channel MOSFET which is driven by a square pulse. The simplicity and low number of components means that it is easy and cheap to fabricate. The primary winding of the transformer is placed in series with the MOSFET.

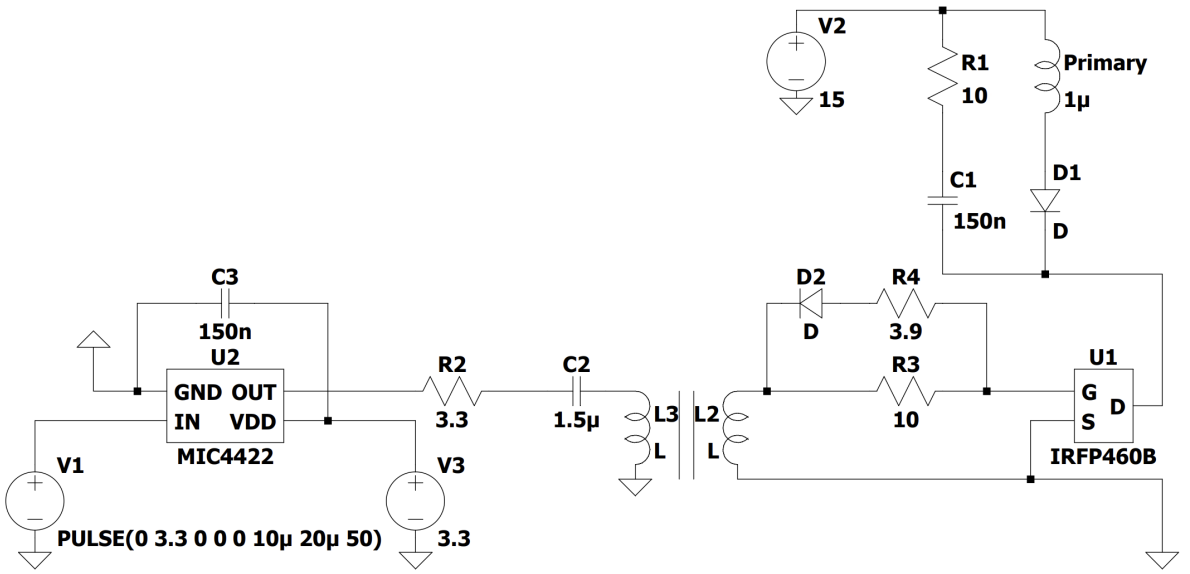

Figure 3.6: Schematic of the Unipolar driver

3.4.1. RC Snubber Circuit

To switch an inductive load like in the case of a transformer, one must take ringing into consideration. Ringing is the phenomenon where the stored energy of the inductor is oscillated between the inductor and its stray capacitance.

When the N-channel MOSFET rapidly opens, the magnetic field in the primary collapses on itself and the stray capacitance is charged up. The value of this capacitance is often in the orders of pico Farads which means that the voltage must increase dramatically to store the energy of the collapsing field as shown in equation 3.2.

$$E_L = E_C \tag{3.1}$$

$$\frac{1}{2}L\mathbf{I}^2 = \frac{1}{2}C\mathbf{V}^2 \tag{3.2}$$

Although these oscillations may quickly decay due to internal resistance, the amplitude of the initial spikes may be much higher than the maximum Drain to source voltage that the MOSFET can handle. Depending on the coil geometry, this may even be in the range of several thousands of volts if no precautions are taken. To protect The MOSFET, a snubber circuit is implemented. This additional circuit is composed of a resistor and a capacitor. From equation 3.2 it can be deducted that by increasing the overall capacitance, the same amount of energy can be stored with a lower voltage. The IRFP460A has a maximum drain to source voltage of 500V. It is common practice to keep the operating voltage under 50 to 80% of this absolute maximum value. For longevity purposes, 250V has been chosen as the maximum safe operating voltage. In steady state, the designed transformer allows a current of 50A to flow. By filling these values into equation , a minimum value of 64nF was obtained for the snubber capacitor. Due to availability, a 150nF film capacitor was used. The fact that the used capacitor is more than twice the calculated value does not matter as this simply means that the voltage will remain lower. Using a snubber capacitor that is several orders of magnitude too large is not advised, as it can result in an excessive inrush current, potentially damaging other components [17]. It is important to use a non-polarized capacitor with a low Equivalent Series Resistance (ESR) such as a film capacitor because this enables it to react quickly.

$$C_{Snub} = \frac{LI^2}{(\frac{V_{Max}}{2})^2} = \frac{1.6 * 10^{-6} * 50^2}{(\frac{500}{2})^2} = 64nF \tag{3.3}$$

3.5. Gate Driver Resistor

When designing a PWM driving circuit it is essential to minimize external parasitic inductance and capacitance between the driver IC and the transistor. This is because of their influence on the gate driving signal and switching speed. The parasitic impedance may introduce a high quality factor (Q-factor) during switching if no precautions are taken. This may also be interpreted as ringing during the on and off switching of the MOSFET. The Q-factor is a dimensionless factor that describes how dampened oscillations are during switching in the case of an RLC circuit. The schematic for this particular circuit can be seen in fig. 3.7. This circuit only contains the parasitic components that can be found inside of the MOSFET. The series driver resistance R_{DRV} is not displayed in this schematic but it should not be ignored during calculations.

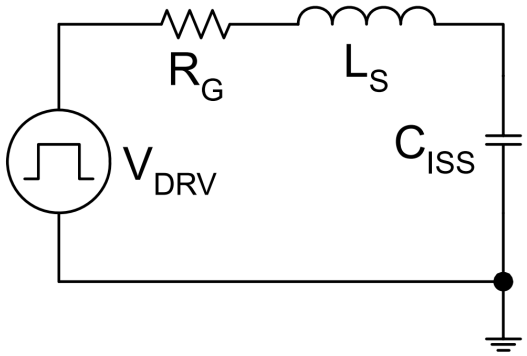

Figure 3.7: Internal MOSFET RLC-circuit [18]

$$Q = \frac{\omega_0}{\Delta\omega} = \frac{\omega_0}{\omega_2 - \omega_1} \tag{3.4}$$

$$\omega_0 = \frac{1}{\sqrt{LC}} \quad , \quad \Delta\omega = \frac{R}{L} \tag{3.5}$$

$$\omega_1 = -\frac{R}{2L} + \sqrt{\left(\frac{R}{2L}\right)^2 + \frac{1}{LC}} \quad , \quad \omega_2 = \frac{R}{2L} + \sqrt{\left(\frac{R}{2L}\right)^2 + \frac{1}{LC}}. \tag{3.6}$$

$$Q = \frac{1}{R_{tot.}}\sqrt{\frac{L_s}{C_{iss}}} \tag{3.7}$$

$$R_{tot.} = R_{G,opt.} + R_{DRV} + R_{G,I} \tag{3.8}$$

$$Q = \frac{1}{R_{G,opt.} + R_{DRV} + R_{G,I}}\sqrt{\frac{L_s}{C_{iss}}} \tag{3.9}$$

The formula for the Q-factor of an RLC series system is given by the ratio between the resonant frequency of the signal and the bandwidth. This is expressed in equation 3.4.

The ideal Q-factor value is considered to be 0.5 for electrical systems as this is the point where ringing is dampened without distorting the signal any more than necessary. To reach this quality factor, an additional gate driving resistor is added in series. The formula to find the resistor value is given by equation 3.10 [19].

$$R_{G,opt} = \frac{1}{Q_{opt.}}\sqrt{\frac{L_s}{C_{iss}}} - (R_{DRV} + R_{G,I}) \tag{3.10}$$

The resistance value for the driver in its high state $R_{G,I}$, is given in the datasheet for the MIC4422 and is $0.6\,\Omega$ The datasheet of IRFP460A MOSFET contains a typical value for the input capacitance of 3200pF. The range of this value was confirmed with the use of an LCR-meter with a measured value of 4684pF. No numerical values for $R_{G,I}$ and L_s are specified in the datasheet [20]. To obtain these values, more complicated methods must be applied. A reasonable value for L_s can be found by using an LCR-meter due to the limited measurement frequencies. Therefore a Vector Network Analyzer (VNA) has been used to find the resonant frequency. The source and drain terminals of a MOSFET were shorted and the connected to the VNA [21]. To convert the resonant frequency reading into an inductance value equation 5.1 was used. Finding a value for the gate input resistance $R_{G,I}$ proved to be much harder due to its small size and the influence that parasitic capacitance may have. It was concluded that this measurement falls outside the scope of this project. This measurement requires the use of a VNA in conjunction with a DC bias injector. The output of this process would look like an impedance vector, from which the real part can be considered the input gate resistance [22].

Due to the difficulty of the input gate resistance measurement, A commonly chosen value of $10\,\Omega$ has been used as the gate driving resistance. This is not an optimal value and may lead to oscillations when switching.

$$f_r = \frac{1}{2\pi\sqrt{LC}} \tag{3.11}$$

Later, a parallel discharging path has been added to the gate driver circuitry to allow for a faster discharging speed. This path consists of a diode in series with a smaller resistance compared to that of the gate charging resistor. In the case of gate discharging, the diode will be forward biased and therefore allow for a high current to flow through the discharging resistor. This is particularly important when switching a half bridge, as one must make sure that the transistor opens up before the closing of the complementary transistor. In the case that this does not happen, and that both MOSFETs are conducting at the same time, a short circuit will take place which would likely damage the switches. By rapidly discharging the gate it is possible to safely use a smaller dead time between switching the complementary switches. Rapidly turning off a MOSFET ensures that the transistor spends the least possible time in its linear conduction region preventing unnecessary heating.

3.6. Bipolar Driver

The bipolar driver is based on two half-bridge circuits creating a full-bridge composed of four N-channel MOSFETs. The PWM generator supplies two complementary pulse signals to two UCC21521 based gate driver boards as shown in figure B.6 by the blue wires going to the black Printed Circuit Boards (PCB). These gate driver boards are for evaluation only and must be redesigned for commercial applications. The full-bridge is able to supply bipolar pulses constantly switching on and off the diagonal MOSFETs in schematic 3.8. when the upper left and down right MOSFET are in their conducting state a current fill flow from the left to the right through the transformer primary. The opposite happens when the top right ans bottom left MOSFET conduct.

The main advantage that a bipolar driver offers for high voltage transformers is that it is an effective way of preventing core saturation. The supplied voltage may effectively be twice as high before reaching the saturation point of the ferrite core. This is because the magnetic flux in the core fill first go to half that of a unipolar driver, go back to zero and then flow in the opposite direction [23].

The design was made modular. This means that the driver is easily disassembled in its individual components, facilitating circuit diagnostics and repairs. A possible disadvantage of this technique are the longer connections between the different modules leading to higher noise levels. This is likely not of great importance as the connections did not exceed 10cm and the highest operating frequency is 100kHz.

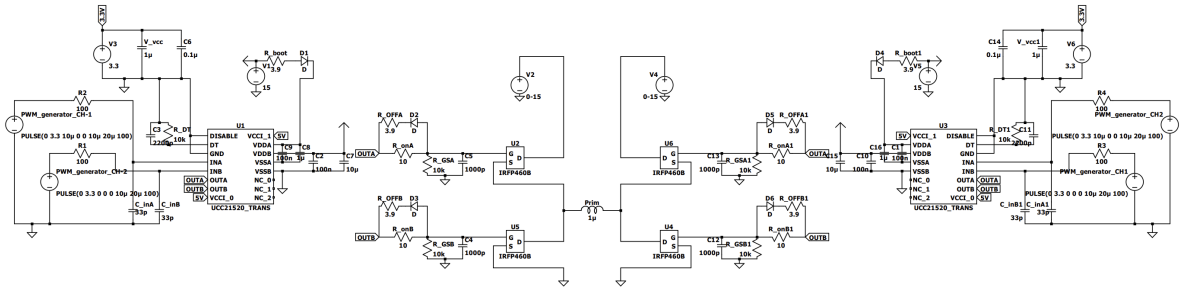

Figure 3.8: Schematic of two half bridge circuits forming a full bridge [24]

3.6.1. Gate Driver Isolation

Implementing a certain level of isolation is essential for driving a high voltage half bridge. The source terminal of the high side N-channel MOSFET is connected to the load rather than ground which means that it is floating compared to the gate terminal. The voltage on the source can therefore be much larger than what a normal gate driver can handle, especially in the case of voltage spikes when switching an inductive load.

To protect the gate driver, two main options are available. The first and oldest method is by coupling a one channel non-isolated gate driver to the MOSFETs through a pulse transformer. A complementary signal can be generated by adding an extra oppositely turned secondary winding. This type of transformer is designed in a particular way to transfer Pulse signals with low distortion. This method is simple and reliable but increases the cost of the design together with making it more prone to noise. Additionally, a gate drive transformer complicates high duty cycle controlled switching due to core saturation. To prevent this, a DC restore circuit can be used but this revokes the main advantage being simplicity [25]. The transformer method has been used for the unipolar driver design but has later been discarded due to its complexity as it was not necessary. The unipolar driver only uses a low side MOSFET but a certain degree of isolation was preferred.

The second option is to use an isolated gate driver which has two channels. This driver contains internal capacitive isolation as show in figure . The UCC21521 driver IC that has been used has a good internal isolation that can withstand 5.7kV. This technique is favorable for high frequency duty adjustable applications and has therefore been applied to the bipolar driver.

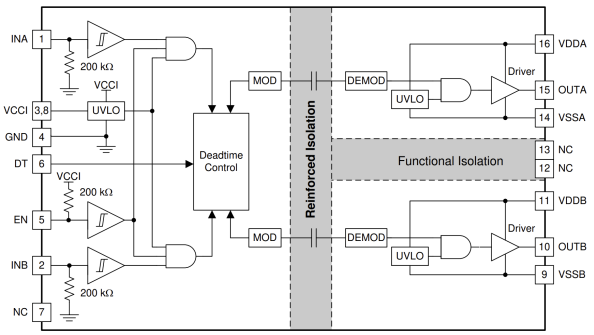

Figure 3.9: Isolation in a half-bridge setup of an isolated gate driver IC (UCC21521) [26]

3.6.2. Bootstrap Circuit

It is common practice to use N-channel MOSFETs for both the low side and the high side of a half bridge. The preference of using two N-channel MOSFETs over a combination of a PMOS and NMOS stems from the fact that electrons have a higher mobility in a semiconductor compared to holes. This means that an NMOS can switch much faster. The lower charge carrier mobility directly relates itself to a higher ON resistance as seen in equation 3.12 [27].

$$R_{\mathrm{DS,\,linear}} = \frac{1}{\mu_n C_{\mathsf{ox}} \frac{W}{L}(V_{\mathsf{GS}} - V_{\mathsf{TH}})} \tag{3.12}$$

[27]

To ensure proper gate charging of an NMOS, V_{GS} must be positive and exceed the threshold voltage V_{th}. The source terminal can easily reach higher voltages than what the gate driver can deliver. To guarantee that the gate voltage is higher, it is possible to use a bootstrap circuit. This circuit is composed of three components being a diode, a capacitor and a resistor. When the low side MOSFET in a half bridge is conducting, the diode will be forward biased meaning that the bootstrap capacitor will be charged as seen in figure 3.10a. The resistor serves to limit the current flow going through the bias circuit. As soon as the low side MOSFET is turned off, the diode will go in reverse bias and the bootstrap capacitor will discharge itself into the high side MOSFET gate though the driver IC as showed in figure 3.10b

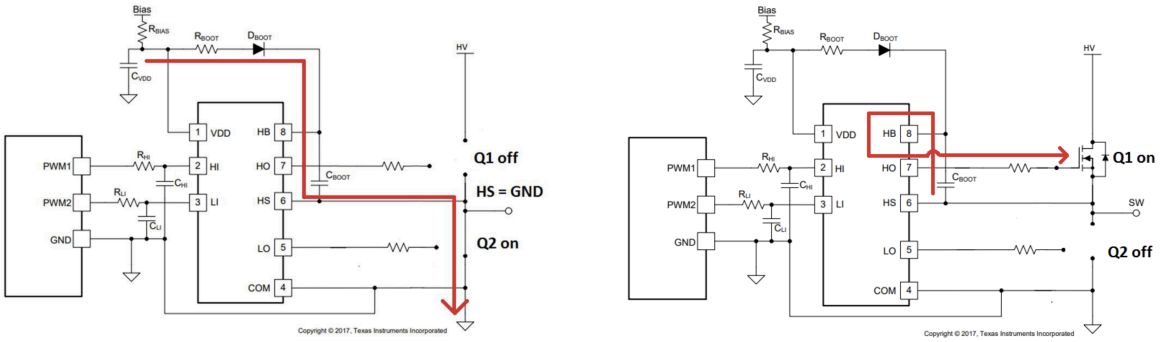

(a) Bootstrap capacitor charging while low-side MOSFET is conducting

(b) Bootstrap capacitor discharging into the gate of the high-side MOSFET

Figure 3.10: Operation of the bootstrap circuit in a half-bridge configuration [28]

4

High voltage pulse transformer

An essential part of a high voltage pulse power supply is an appropriate pulse transformer. This type of transformer differentiates itself by being able to transfer pulses with very little distortion. Additionally, the transformer must amplify the voltage, so as to obtain high voltage peaks, up to 10 kV and it should be able to operate from 10kHz up to 100kHz.

4.1. Pulse waves vs. sine waves

The behavior of the transformer is defined by Ampère's law and Faraday's law (4.1 and 4.2 respectively). The current through the primary coil induces a magnetic field through the core. After that, the changing magnetic flux induces an electromotive force on the second coil.

$$\oint \vec{B} \cdot d\vec{l} = \mu_0 I \tag{4.1}$$

$$\epsilon = -\frac{N d\phi}{dt} \tag{4.2}$$

4.2. Transformer characterization

As stated in the technical requirements, a frequency range of 10 kHz up to 100 kHz is desired. This requirement influences the transformer design drastically. Further, the standard IEEE 390 model is used to model the behavior of the pulse transformer [29].

To extract all the parameters accurately, the Bode 100 vector network analyzer (VNA) was used. The Bode 100 has one output and two inputs. Two different types of measurements are executed to characterize behavior of the transformer. One of them is the one-port measurement. The one-port measurement is designed to perform quick impedance, admittance and reflection measurements.

The second type of measurement that is used is the gain/phase measurement. This measurement is used to measure the transfer function of filters and other circuits.

The output terminal is used to sweep an AC signal with frequency starting from 1 Hz up to 40 MHz. Input channels 1 and 2 measure the voltage and are synchronized with the output signal of the Bode 100. In this way the magnitude and phase relation between the output signal and the input signals can be within the frequency range. Using the magnitude and phase ratio between the two voltages, the Bode 100 calculates the complex gain values of the device under test (DUT) [31].

4.2.1. R_1 and R_2

R_1 and R_2 can be measured with the DC setting. A 4 wire sensing setup should be used for very low winding resistances. If the real part of the impedance is not too low compared to the imaginary part of

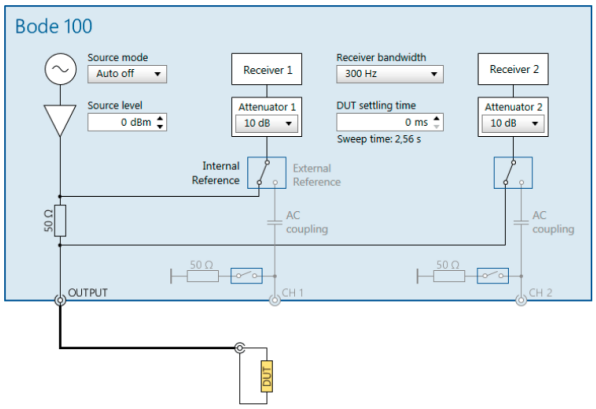

Figure 4.1: Internal setup for a one-port measurement [30]

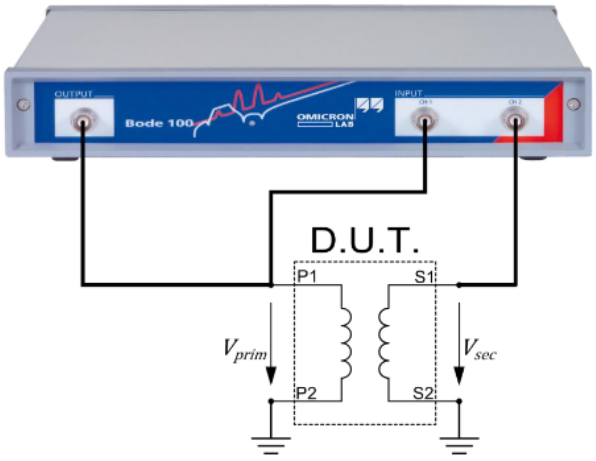

Figure 4.2: Setup for a gain / phase measurement [30]

the impedance, the measurement of the winding resistances R_1 and R_2 can be performed by the Bode 100.

The winding resistances can be measured by the one-port measurement on the Bode 100. If the winding resistance of the primary coil is of interest, the V+ terminal is connected to one side of the coil, and the ground terminal to the other side of the coil and the secondary coil open circuit. The equivalent circuit in case that the secondary coil is open can be seen in figure 4.4.

For this measurement it is essential that the start frequency of the sweep is as low as possible. In this way the influence of the parasitic capacitors small. Additionally, the signal level should be small to minimize the influence of the core resistance R_C. The core resistance R_C is highly dependent on the frequency and the magnetic flux density inside the core.

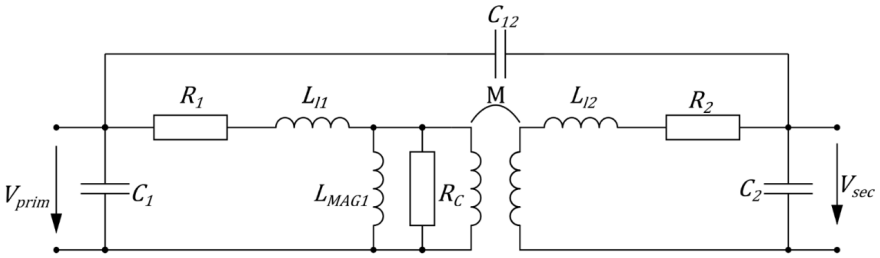

Figure 4.3: Equivalent model of a transformer [30]

Measuring the secondary winding resistance R_2 is done in a similar way. Instead of connecting the primary coil to the VNA and leaving the secondary coil open circuit, the primary coil should be left open circuit and the secondary coil should be connected to the VNA. The sweep settings should be left the same to minimize the core losses R_C.

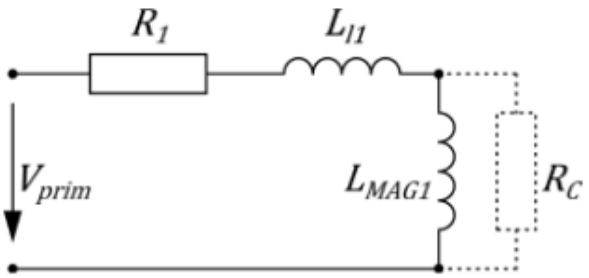

Figure 4.4: Equivalent circuit when the secondary coil is open [30]

4.2.2. L_{l1}, L_{l2}, L_{MAG1} and L_{MAG2}

The measurements of L_{l1}, L_{l2} and L_{MAG1} require a bit more steps than the measurements of R_1 and R_2. Firstly, a similar measurement to those of the resistances, must be executed to find the inductances. Just like the measurements to find the winding resistances, the primary coil should be connected to the VNA and the secondary coil should be left open. The inductance has to be measured at a frequency where the inductance is stable and before the inductance starts to decrease significantly. It is important to note this frequency down. The measured inductance is the sum of the primary leakage inductance L_{l1} and the primary magnetizing inductance L_{MAG1}. Next the secondary coil should be connected to the VNA and the primary should be left open circuit. Again, find the inductance at a frequency where it is stable and before it starts decreasing significantly. Note this frequency and inductance down. The measured inductance is the sum of L_{l2} and L_{MAG2}.

At the moment the sum of the leakage and the magnetizing inductance is known. The next step is to either find the leakage inductance or the magnetizing inductance. It is the easiest to find the magnetizing inductance. For this, a gain measurement should be performed. The secondary winding should be connected to both the output and to channel 1 and the primary winding should be connected to channel 2. The setup has to be in this order to prevent over voltage on channel 2. Measure the gain at which the frequency L_1 is measured and calculate L_{MAG2} using the following relation with $a = \frac{N_1}{N_2}$ (turns ratio).

$$G = \frac{|V_{CH1}|}{|V_{CH2}|} = \frac{\omega L_{MAG2}}{\sqrt{R_2^2 + (\omega L_2)^2}} a$$

4.2.3. C_{12}, C_1 and C_2

The interwinding capacitance C_{12} can be measured by shorting both the primary coil as the secondary coil. A one port measurement is taken with a sweep in the higher frequency range starting from 10 kHz and ending at the maximum possible frequency which is 40 MHz if the Bode 100 VNA is used. The interwinding capacitance C_{12} should be measured in a frequency range where the capacitance is stable.

The method to calculate the individual interwinding capacitances C_1 and C_2 require a bit more steps. To measure the primary interwinding capacitance C_1, secondary coil should be short-circuited and the one end of the primary coil should be connected to the secondary coil. The equivalent circuit is visible in figure 4.5.

A gain/phase measurement is executed and the resonant frequency should be recorded (frequency where the gain is at its maximum). Using figure 4.5, the relation between the resonant frequency, C_{C1} and L_{C1} can be derived, resulting in 4.5 [32]. Combining equations 4.5,4.3 and 4.4 in combination with $n = \frac{n_1}{n_2}$, the winding capacitance C_{C1} can be calculated.
The interwinding capacitance C_{C2} can be calculated in a similar manner as C_{C1}. Instead of shorting the secondary coil with one end of the primary coil, the setup is reversed. The primary coil should be shorted

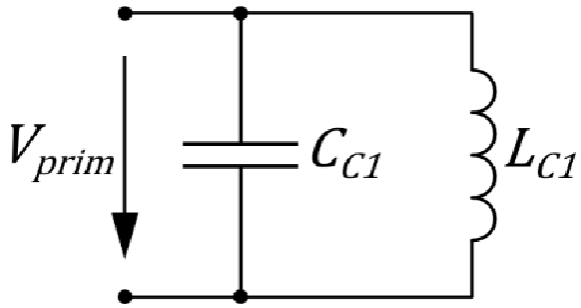

Figure 4.5: Equivalent circuit when secondary coil is short-circuited with one end of the primary coil [30]

with one end of the secondary coil. Again a gain/phase measurement is executed and the resonant frequency should be measured. In equations 4.5,4.3 and 4.4, the inductances and capacitances will change accordingly ($L_{MAG1} -> L_{MAG2}$ etc.). Additionally, $n = \frac{n_2}{n_1}$ will be used.

For the sake of simplicity the influence of the core resistance is ignored. It is assumed that the core resistance is large enough to have a significant influence on the behavior of the transformer [31] [29] [33] [29] .

$$C_{C1} = C_1 + C_{12} \tag{4.3}$$

$$L_{C1} = L_{l1} + \frac{L_{MAG1} \cdot n^2 L_{l2}}{L_{MAG1} + n^2 L_{l2}} \tag{4.4}$$

$$2\pi f_{resonant} = \frac{1}{\sqrt{C_{C1} L_{C1}}} \tag{4.5}$$

4.3. Pulse Transformer Design

One constraint of transformers that is not yet mentioned is core saturation. This occurs when the magnetic flux through the core no longer increases proportionally with the primary current. In other words, the core becomes 'saturated' with magnetic flux.

The maximum current before core saturation limitations for pulse waves are given by equation 4.6. N_1 is the number of turns at the primary coil, I_sat is the saturation current at the primary coil, B_{max} is the maximum magnetic induction of the magnetic core material, l_e is the effective length of the magnetic core and μ_r is the relative permeability [34].

$$N_1 I_{sat} = \frac{B_{max} l_e}{\mu_0 \mu_r} \tag{4.6}$$

The equation above can be rewritten into equation 4.7. This formula relates the maximum output voltage to the frequency, turn ratio, area and the saturation flux density.

$$V = N \cdot A_c \cdot \frac{dB}{dt} \tag{4.7}$$

For pulses the equation 4.7 results in $V_{sat} = 4 \cdot f \cdot N \cdot A_c \cdot B_{max}$ [35]. The maximum voltage level on the primary coil is limited by frequency, area, maximum magnetic flux density and number of turns. Since a minimal frequency of 10 kHz is desired and a maximal voltage level of 10 kV, the biggest transformer core available with an area of $7.07cm^2$ was used. The decision was made to use a ferrite transformer core because of its low energy loss, cost, thermal characteristics and fairly good core [23]. However, this core is not able to operate at 10kHz. Therefore the goal was set to have minimal operating frequency of 20kHz.

Like discussed earlier, by keeping the parasitic elements as small as possible, the transformer is able to generate pulse waves with a better accuracy at the output. According to Lagerweij(2024) [36]: ”The parasitic elements: leakage inductances L11 and L21 and parasitic capacitances C11 and C22 limit the bandwidth of the transformer. Resonances between these elements can result in overshoot and high□frequency ringing when driven by a rectangular pulse.” A high bandwidth of the transformer results in fast rise times at the transformer’s output.

Elements R_1 and R_2 can be minimized by using wire with a low resistivity, big area and small length on the primary coil and secondary coil.

$$R = \frac{\rho L}{A}$$

To minimize the parasitic elements L_{l1}, L_{l2} the number of turns on both the primary and secondary coil should be small. Moreover the According to Erickson(2001) [37] the following holds.

$$L_{leakage} \propto \frac{N^2 \cdot \text{mean turn length} \cdot \text{winding separation}}{\text{winding height}}$$

According to Paul(2006) [38] the interwinding capacitance in multi layered coil could be approximated by the following equation.

$$C_{interwinding} \approx \frac{4\pi\epsilon_0\epsilon_r N D}{3}$$

As can be seen in the formulas both the leakage inductance and interwinding capacitance decrease with a lower number of turns. Moreover the leakage inductance is minimized by coupling the windings tightly while the interwinding capacitance is minimized by using spacing and shielding between the turns. This opposes each other and therefore an optimal trade-off between the two has to be found while still taking core saturation into consideration. Therefore the design steps in figure 4.6 were executed where each design was characterized. Finally, in the design process of the transformers, arc prevention should be taken into consideration. When a large voltage difference occurs between the different windings and the windings are close/in contact with each other, an arc will form between the two turns and the transformer will break. Wire with thick isolation can be used but another solution is to make different isolated compartments. In this way no big voltage differences will be over two directly neighboring turns.

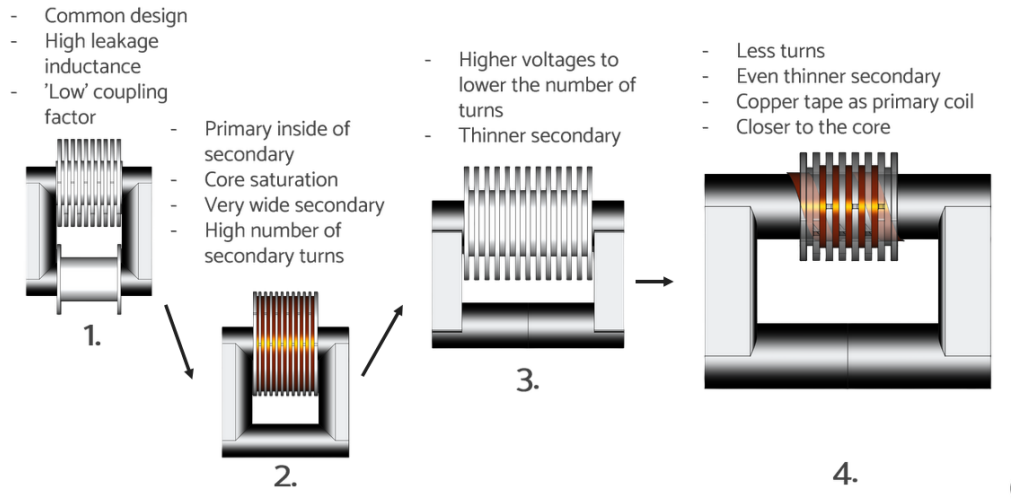

Figure 4.6: Design steps for a pulse transformer

5

Results

The Unipolar driver was built and tested. After powering on the circuit the gate driver IC overheated due to unknown reasons. This meant that no measurements could be taken with this circuit. The bipolar driver was tested with three different loads in combination with a self made pulse transformer UY30;1.5;392;5. All tests were done with a 50% duty cycle. The transformer codes that are used are formatted in the following manner:
(Core size; # Primary turns; # Secondary turns; # Isolated compartments)

5.1. Bipolar driver results

The gate driver modules were initially tested without the MOSFETs. This was done as a safety precaution to ensure that the complementary PWM signals did not overlap. Both of the half bridge driver modules operated with no problems as seen in figure B.7. Additionally, the complementary gate signals were measured at a frequency of 100kHz and are plotted in figure B.8. The dead time in the PWM generator was set at 2µs and the factory dead time of UCC21521 gate drive modules was left at 100ns.

The first load that was connected was a fractal electrode, milled on a both sides of a copper clad laminate board 5.2 [39]. This load had a large capacity of 236pF due to the small spacing between the electrodes and the overall large combined surface area of the fractal lines. This large capacity directly correlates to a lower impedance of the load, therefore drawing more current. The MOSFETs on the bipolar driver quickly reached a temperature of well over 60°C. The large capacitive load deformed the output voltage into a sine waveform as seen in figure 5.1. The power supply feeding the driver circuit went into current overload protection at 5.36A with an peak to peak output voltage of 6kV. This meant that no higher output voltages could be tested with this load and no substantial amount of plasma byproducts were produced. This electrode required a powerful HV power supply such as a ZVS driver to run extended periods of time [4]. As discussed in chapter 2, using a sine wave power supply is not an efficient way of generating cold plasma,as it leads to excessive heating of the electrode.

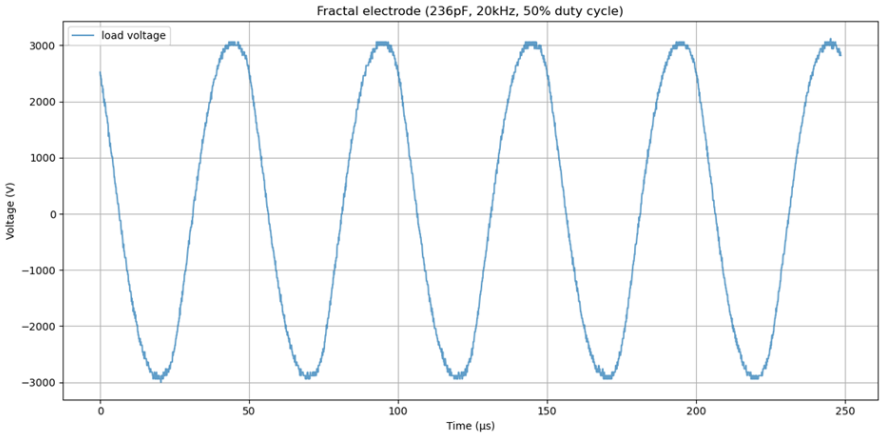

Figure 5.1: Milled fractal electrode load voltage measurement (pk-pk voltage= 6kV, load= 236pF, freq.20kHz, duty cycle = 50%)

To test the PAW producing capability of the High voltage power supply, a small test setup was built from two Petri dish covers as seen in figure 5.3. The testing setup is of the non-thermal DBD type which means that a dielectric is placed in between the electrodes to prevent arcing. Distilled water was poured in the bottom plate which contained several wire electrodes above it. A capacity of 18pF was measured with an LCR-meter for the Petri dish setup.

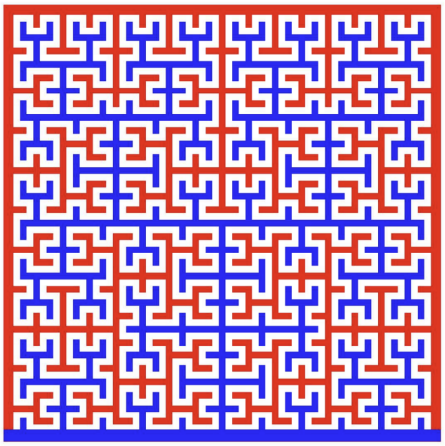

Figure 5.2: 5th order Hilbert electrode [39]

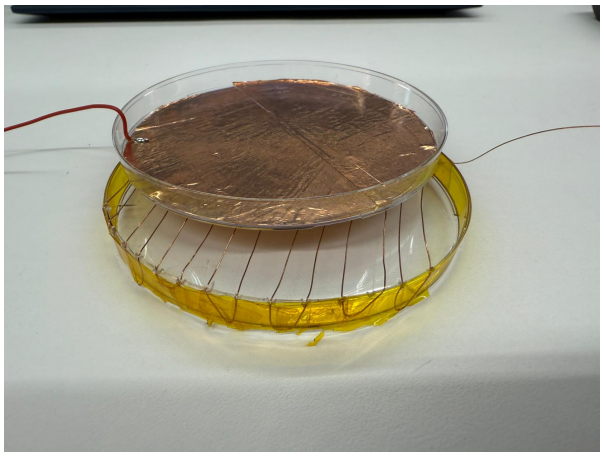

Figure 5.3: Petri dish DBD setup

The bipolar driver in combination with the (UY30;1.5;392;5) transformer design were able to successfully create PAW. The power supply was able to supply a close to square pulse due to the relatively low capacitive load of the dish setup as seen in figure 5.4. The distilled water started with a pH of 7.86 and reached a level of 2.94 in approximately 20 minutes. A peak to peak output voltage of 7.6kV with a frequency of 20kHz and a duty cycle of 50% was used to treat the water. The MOSFETs during this test did not exceed a temperature of 35 degrees with a 16cm^2 aluminum sheet for each switch. Higher loads may require bigger heat sinks or active cooling. The input voltage of the bipolar driver was set to 10.9V and drew a current of 1.11A meaning that the power supply can easily generate PAW using only 12W.

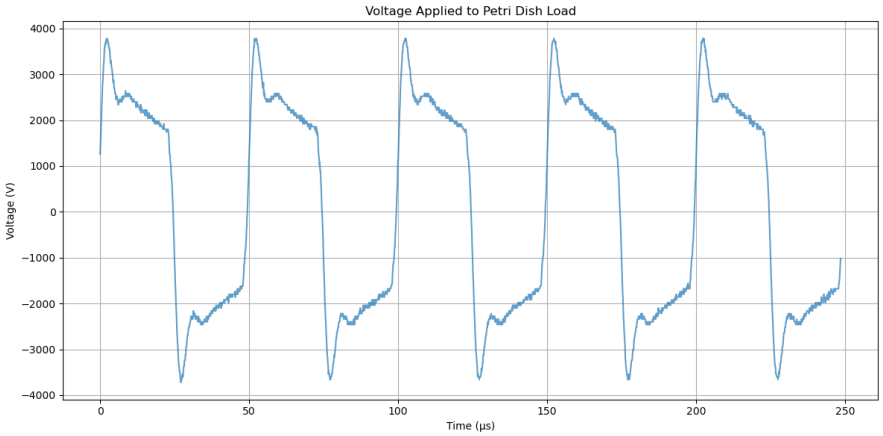

Figure 5.4: Voltage measurement in parallel to the Petri dish load (pk-pk voltage= 7.6kV , freq.= 20kHz, duty cycle = 50%)

The spikes that can be seen at the beginning of each cycle in figure 5.4 are likely related to a small time constant of the transformer primary winding. When current begins to flow through the primary coil, it reaches its steady state too quickly, causing the output voltage on the secondary side to sag [40]. The formula for the time constant is given by equation 5.1 [41]. From this formula it can be concluded that to increase the time constant two options are available. Firstly, by increasing the number of turns on the primary coil it is possible to increase its inductance. Despite being effective, this is not favorable as it would worsen the pulse transformer and deform the wave. The second option is to lower the primary coil resistance.

$$\tau = \frac{L}{R} \tag{5.1}$$

To conclude, a triple coaxial load was tested which was designed and built by the plasma generation subgroup. The testing setup is shown in figure B.11. This load had a capacitance of 87.5pF, which is much higher than that of the Petri dish setup. The Power consumption has been measured at different load voltages and plotted in figure 5.5. This was repeated for two other smaller commercial high voltage transformers. A clear difference is visible for the UY20;6;1000;10 transformer. This is because the operating frequency of 20kHz is close to the resonant frequency of the secondary LC tank circuit. By filling in the secondary leakage inductance of 1.129H and the load capacitance into the resonant frequency equation , a frequency of 16kHz is obtained. Although this is more efficient, operating at the resonant frequency would mean that the output voltage becomes a sine wave. The self made transformer was able to supply the triple coaxial load with 8kV while consuming only 25W.

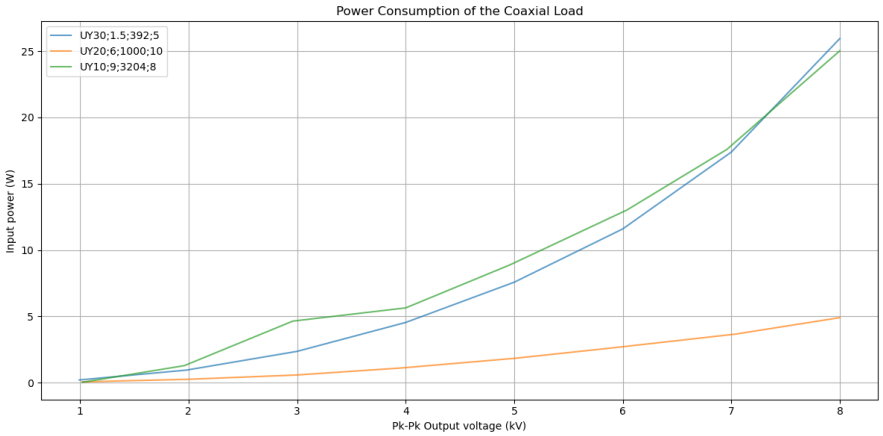

Figure 5.5: Power consumption of three different transformers at different output voltages (Triple coaxial load: 87.5pF, freq.= 20kHz, duty cycle= 50%)

Increasing the output voltage above 8.5kV resulted in a loud high pitch sound. The transformer was therefore not tested at a higher voltage with the coaxial load. The sound might have been caused by vibrations of the transformer but this must be further examined. Moreover, the transformer's secondary coil is not casted in resin, meaning that it will likely arc if the voltage is increased.

5.2. Transformer results

Multiple transformer designs have been made and characterized during the project. Additionally, two commercial transformers have been tested and compared to the final transformer design (UY30;1.5;392;5). The waveforms of three transformers have been measured and plotted in figure 5.6 for comparison. These measurements were taken with the bipolar driver circuit and the same triple coaxial load. The designed pulse transformer offers the most pulse-like output waveform.

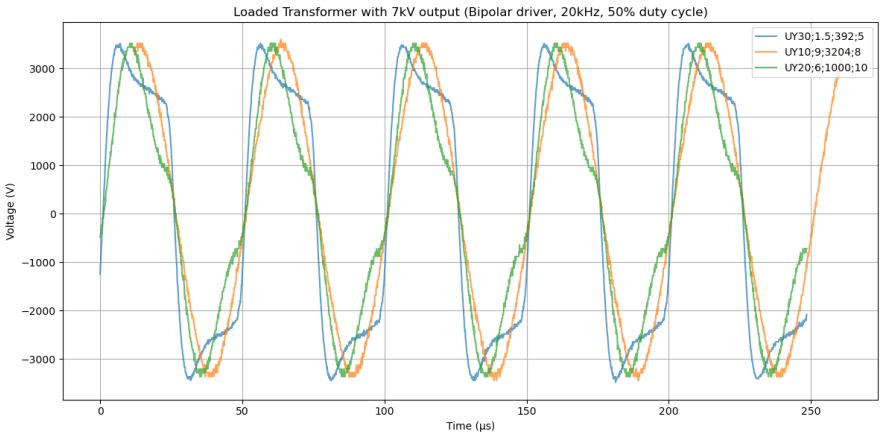

Figure 5.6: Output waveform for three different transformers with the Bipolar driver (pk-pk voltage= 7kV, freq.= 20kHz, duty cycle= 50%)

5.2.1. Characterization

Different transformers were characterized differing in size, turn ratio and amount of isolated compartments on the secondary coil. Different transformer designs are given in Appendix C.

The parasitic elements were measured like discussed in section 4.2 and the results are given in table 5.1.

Table 5.1: Characterization of different transformers.
Transformer Model code: (Core size;Primary turns;Secondary turns;Isolated sections(;Tape Primary))

Transformer Model	Parameters									
	R_1 $[\Omega]$	R_2 $[\Omega]$	C_{12} $[F]$	C_1 $[F]$	C_2 $[F]$	L_{leak1} $[H]$	L_{MAG1} $[H]$	L_{leak2} $[H]$	L_{MAG2} $[H]$	$\frac{N_2}{N_1}$ $[-]$
UY20;6;1000;10	542m	48.4	75.7p	0p	0p	58µ	1.5µ	1.129	43µ	$\frac{1000}{6}$
UY20;1;1440;6	450m	90.5	23p	3.45p	136.262p	25.12µ	2.9214µ	200m	6.05	$\frac{1440}{1}$
UY30;1.5;392;5	148m	26.42	88.6p	0p	15.56n	18.36µ	1.63755µ	555.6m	111.84m	$\frac{392}{1.5}$
UY30;1.5;392;7	92m	26.17	90.7p	0p	151n	21.267µ	1.2327µ	543.24m	84.189m	$\frac{392}{1.5}$
UY30;1.5;392;5;T	707m	27	44p	1.6p	0.54p	9.45µ	1.31µ	295m	892m	$\frac{392}{1.5}$

Comparing the characterization results of the different transformers, transformer UY30;1.5;392;5;T was selected. Like discussed in 4, the most important characteristics of a pulse transformer are its low interwinding capacitance and leakage inductance. While transformer UY30;1.5;392;5;T is larger than the UY20 transformers, the performance of the transformer is higher and that is the prioritized in this project.

6 Discussion

During the project, multiple modules were built which together formed a working high voltage pulse power supply. The final product includes the Pulse generator, the bipolar driver and the UY30;1.5;392;5 pulse transformer. The power supply meets the majority of the initial requirements that were set with the exception of the operating frequency and the voltage range. During the design, different compromises were made with the main one being the increase of the minimum operating frequency to 20kHz. This was done to prevent current saturation while still maintaining a high enough voltage to create PAW. The power supply is currently unable to supply 10kV because the transformer is not yet casted.

The power supply was successful in making PAW at a small scale but has difficulty to drive large loads while keeping its pulse waveform. This result indicates towards a modular final design that is built out of many many smaller pulse power supplies. Multiple smaller coaxial loads may be placed next to each other and powered separately by their own power supply. This would make the final to scale setup safer compared to one large and powerful power supply. An added benefit would be the increase in reliability as a faulty power supply would not be detrimental to the overall functioning of the PAW generator. This means that a for scalability purposes, a segmented setup as shown in figure B.13 might be worth pursuing.

6.1. Future improvements

Time constraints have limited the number of improvements that could be made to the designs. Several methods may be used to further improve the performance of the designs.

6.1.1. Improvements on the Unipolar Driver

As a result of time restrictions and a priority shift in favor of the bipolar driver circuit, the unipolar driver circuit was set aside. Future suggestions include:

- The gate input resistance of the MOSFET could be measured such to calculate the optimal gate drive resistance.
- The circuit currently does not use the gate drive transformer as this was not necessary for a pull down N-channel MOSFET. This was done to simplify the circuit during the debugging process. The transformer could be reintroduced to galvanically isolate the PWM generator from higher voltages.
- A better gate driver could be used with an enable function. This would be used to add features like over-current or over-voltage protection.

6.1.2. Improvements on the Bipolar Driver

- The efficiency of the H-bridge may be increased by replacing the Silicon MOSFETs with a more efficient technology like Silicon Carbide MOSFETs. These transistors have a lower ON-resistance and switching losses.

- The circuit could be converted into a zero voltage switching (ZVS) circuit. This would lead the MOSFETs to switch when their drain to source voltage is zero.
- The current circuit only uses a four small aluminum plates which are bolted to the MOSFETs with thermal paste. This configuration may overheat for higher loads or longer operations. Bigger heat sinks or active cooling should be used. Another improvement that may be necessary to reliably operate the power supply for extended periods of time may be a temperature protection circuit.
- The HV pulse power supply currently requires a high voltage measurement probe and an oscilloscope to choose the output voltage. To make the power supply more user-friendly and more accessible to less experienced operators, a built-in high voltage measurement stage should be added with a display. This can be done by building a 1/1000 voltage divider with high voltage resistor and a tuning circuit so that it can operate on higher frequencies.

6.1.3. Improvements on the pulse transformer

- The primary coil admittance should be increased to increase the time constant of series RL-circuit. By keeping the inductance of the primary coil smaller it is possible to prevent the use of a large number of windings on the secondary coil. Therefore, it is only possible to adjust the time constant by the tweaking the resistance of the primary coil. This can be done by using a thicker wire or multiple layers of copper tape depending on the design.
- Changing the design of the secondary coil to a single layer. This means that copper winding do not cover each other, thus lowering the parasitic capacitance of the secondary coil. lowering these capacitance will increase the reaction speed leading to less deformation. Attention must be paid to prevent the length from increasing too much as this may increase the leakage inductance of the transformer.
- Thinner isolation slots may be used to shrink the length of the secondary winding. This might have a positive effect in lowering the leakage inductance. The current isolation slots are 2.5mm thick and made of SLA resin. This can probably lowered to 1-0.5mm, depending on manufacturing tolerances.
- To decrease the required turn ratio, it is possible to increase the voltage that is supplied to the primary winding of the transformer. This lowers the required number of secondary windings to reach the same output voltage. This can lead to a reduction in the parasitic capacitance of the secondary coil. When increasing the voltage on the primary coil, a bigger core of higher frequency must be used to prevent core saturation.
- The secondary windings of the high voltage transformers must be redesigned. This is because the enameled wire comes in contact with higher potential windings when crossing into a different isolated section.
- The high voltage has not yet been casted in epoxy resin or placed in mineral oil. This is necessary to achieve a higher output voltage without arcs forming. Mineral oil contrary to epoxy resin may also benefit the heat dissipation of the transformer.

7

Conclusions

A high voltage bipolar pulse power supply, used for plasma-activated water generation in seed disinfection applications, has been designed and tested successfully in this project. A Mazilli ZVS driver with transformer, a high voltage switching supply using a cascode, a unipolar driver with pulse transformer and a bipolar driver with pulse transformer, were compared, regarding performance, reliability, and cost. The decision was made to make a power supply consisting of a bipolar pulse driver and a pulse transformer. To have an optimal ozone generation, the system was designed to operate from 0 up to 10kV and from 20kHz up to 100kHz. Moreover, the power supply must be reliable and should be able to drive capacitive loads in the pico farad range.

A bipolar driver was designed bearing in mind reliability and efficiency. Additionally multiple custom transformers were designed and characterized, varying in turns ratio, dimensions and number of isolated compartments. The custom transformer (UY30;1.5;392;5) was found to meet the requirements the best. The custom transformer was compared with commercial transformers performance wise. The custom transformer was able to generate a bipolar pulse-like output waveform while the commercial transformers distorted the signal drastically leading to a sinusoidal output waveform. Both transformers had a capacitive load connected of 23 pF.

Future improvements should focus on minimizing parasitic elements of the pulse transformer even further. Moreover, the influence of casting the pulse transformers into resin or mineral oil should be researched. Future improvements for the driver should focus on enhancing thermal management and switching efficiency. Implementing user-friendly features like built-in voltage measurement and display would also improve practicality.

In conclusion, this project provides a solid foundation for small-scale power supply used for PAW generation, with potential for scalability and further refinement. The results align with the goal of offering a bipolar power supply that is able to drive capacitive loads in the pico farad range. The power supply in combination with the products of the other subgroups offer a sustainable alternative to traditional seed disinfection methods, contributing to advancements in agricultural technology. Future work should address the noted limitations to achieve higher voltages and broader operational ranges, ensuring robust performance for industrial applications.

References

1. Thorsen, M. *et al.* Megatrends and emerging issues: Impacts on food safety. *Comprehensive Reviews in Food Science and Food Safety* **24,** e70170 (May 2025).
2. Mancini, V. & Romanazzi, G. *Seed treatments to control seedborne fungal pathogens of vegetable crops* 2014.
3. Peťková, M. *et al. The Effects of Cold Atmospheric Pressure Plasma on Germination Parameters, Enzyme Activities and Induction of DNA Damage in Barley* 2021.
4. B. Salar, Z. H. *High voltage generator for eco-friendly plasma-disinfection of seeds* (Delft University of Technology, 2024).
5. Yücel Kurt, H., Ongun, E. & Utaş, S. The Study of DC□ and AC□Driven GaAs□Coupled Gas Discharge Micro Plasma Systems: Modeling and Simulation. *Journal of Electronic Materials* **53** (May 2024).
6. Wei, L. *et al.* Current pulses and their influences on ozone production in oxygen-fed dielectric barrier discharge. *Journal of Electrostatics* **119,** 103748. ISSN: 0304-3886. https://www.sciencedirect.com/science/article/pii/S0304388622000766 (2022).
7. eeeguide. *eeeguide* https://www.eeeguide.com/paschen-breakdown/.
8. Murata Manufacturing Co., L. *EMI Filter (EMIFIL) Knowledge: Pages 26–30* Murata. https://www.murata.com/~/media/webrenewal/products/emc/emifil/knowhow/26to30.ashx.
9. Montrose, M. I. *EMC and the Printed Circuit Board: Design, Theory, and Layout Made Simple* 1st. Focuses on common-mode chokes in EMI filtering. Chap. 8. ISBN: 978-0-7803-4703-1 (IEEE Press / Wiley, 1999).
10. Zhang, Y. & Wang, H. High-Frequency Modeling of Common-Mode Chokes for Power Electronics. *IEEE Transactions on Electromagnetic Compatibility* **62,** 872–881 (2020).
11. M.DE Semiconductor. *What is a Thyristor? Types of Thyristors and Their Uses* https://mdesemiconductor.com/what-is-a-thyristor-types-of-thyristors-and-their-uses/.
12. PPI UK. *Thyristor Controller Firing Methods* https://www.ppi-uk.com/news/thyristor-controller-firing-methods/.
13. DigiKey. *Home Lighting Controllers Offer Dimming Compatibility* https://www.digikey.com/en/articles/home-lighting-controllers-offer-dimming-compatibility.
14. OVAGA. *BTS7960 Motor Driver Datasheet and Circuit Diagram* https://www.ovaga.com/blog/transistor/bts7960-motor-driver-datasheet-and-circuit-diagram.
15. *L298N Motor Driver Datasheet* Handsontec (2023). https://www.handsontec.com/dataspecs/L298N%20Motor%20Driver.pdf.
16. Al-neamy, S. & Sulyman, S. A. Generation of non- thermal plasma jet using ZVS Driver with flyback transformer. **17,** 1879–1895 (June 2021).
17. Todd, P. C. *Snubbing Methods* SLUP100 - Application Report. Texas Instruments. https://e2e.ti.com/cfs-file/__key/communityserver-discussions-components-files/234/Snubbing-methods-slup100.pdf.
18. TECH$_{WEB}$. *Resonant Circuits: Resonant Frequency and Q Factor* https://techweb.rohm.com/product/power-device/si/18332/.
19. Texas Instruments. *Estimating MOSFET Parameters from the Data Sheet* [Online]. Available: https://www.ti.com/lit/ml/slua618a/slua618a.pdf (2022).
20. Vishay Siliconix. *IRFP460A Power MOSFET* 91234. [Online]. Available: https://www.vishay.com/docs/91234/irfp460a.pdf (Jan. 2022). (2023).

21. Texas Instruments. *Estimating MOSFET Parameters from the Data Sheet* [Online].Available: https://www.ti.com/lit/ml/slup170/slup170.pdf (2022).
22. Picotest. *Measuring MOSFET Gate Resistance* Picotest. https://www.picotest.com/measuring-mosfet-gate-resistance/.
23. McLyman, C. W. T. *Transformer and Inductor Design Handbook* 4th ed. Chapters 3 and 5 discuss core saturation and bipolar vs. unipolar drive advantages. ISBN: 978-0824753936 (CRC Press, 2004).
24. *UCC21520EVM-286 Isolated Dual-Channel Gate Driver Evaluation Module User's Guide* SLUUBG8C. User's Guide (2021). https://www.ti.com/lit/ug/sluubg8c/sluubg8c.pdf.
25. Mazany, A. *Why use a Gate Drive Transformer?* Application Report SLLA602 (Texas Instruments, 2024). https://www.ti.com/lit/an/slla602/slla602.pdf.
26. *UCC21521 4-A, 6-A, 5.7-kVRMS Isolated Dual-Channel Gate Driver with Enable* Datasheet SLUSCO3B (Texas Instruments, 2021). https://www.ti.com/lit/ds/symlink/ucc21521.pdf.
27. Fu., J. *Understanding Buck Power Stages in Switchmode Power Supplies* Application Report SLVA771 (Texas Instruments, 2016). https://www.ti.com/lit/an/slva771/slva771.pdf.
28. Diallo, M. *Bootstrap Circuitry Selection for Half-Bridge Configurations* Application Report SLUA887A (Texas Instruments, Aug. 2018). https://www.ti.com/lit/an/slua887a/slua887a.pdf.
29. IEEE Standard for Pulse Transformers. *ANSI/IEEE Std 390-1987,* 1–32 (1987).
30. *Transformer modelling* Online user manual; accessed Tuesday 1st July, 2025. OMICRON Lab (2017). https://www.omicron-lab.com/fileadmin/assets/Bode_100/ApplicationNotes/Transformer_modelling/App_Note_Transformer_modelling_V_2_0.pdf.
31. *Bode 100 user manual* ENU 1006 05 03. Vesion 6.0. omicron lab (2017).
32. White, J. F. in *High Frequency Techniques: An Introduction to RF and Microwave Design and Computer Simulation* 59–77 (Wiley-IEEE Press, 2004).
33. Passive components. *Transformer Calculation, Losses, Leakage Inductance and Applications* https://passive-components.eu/transformer-calculation-losses-parasitives-and-applications/.
34. Laplace, F. *Pulse Transformer Design Guidelines* Application Note AN-00371-13. Version rev1B (X-REL Semiconductor, Mar. 28, 2014). https://www.easii-ic.com/wp-content/uploads/2021/08/EASii-IC-AN-XTR40010-Pulse-Transformer-Design-Guidelines-AN-00371-13.pdf.
35. Mohan, N., Undeland, T. M. & Robbins, W. P. *Power Electronics: Converters, Applications, and Design* 3rd. Explicit derivation of $V_{rms} = 4.44 \cdot f \cdot N \cdot A_c \cdot B_{max}$ for sinusoidal excitation., 499. ISBN: 978-0-471-22693-2 (Wiley, 2003).
36. Gijs, L. & Mohamad, G. N. Design of a high□frequency transformer based on amorphous cut cores for insulation breakdown testing. *IET High Voltage* (2024).
37. Erickson, R. W. & Maksimović, D. *Fundamentals of Power Electronics* 2nd. DOI: 10.1007/b100747. ISBN: 978-0-7923-7270-7 (Springer, 2001).
38. Paul, C. R. *Introduction to Electromagnetic Compatibility* 2nd. DOI: 10.1002/0471755000. ISBN: 978-0-471-75500-5 (Wiley, 2006).
39. Buitink, C. & Lohman, J. *Plasma DBD Electrodes for a Seed Disinfection Fluidized Bed Reactor* Thesis committee: Prof. dr. ir. J. van Turnhout, Dr. ing. H. van Zeijl, M.D. L. Wymenga, Dr. ir. A. van Genderen. Bachelor's Thesis (Delft University of Technology, Delft, The Netherlands, June 2024). http://repository.tudelft.nl/.
40. Ahmad, A. *Understanding RL Circuit Operation and Time Constant* https://eepower.com/technical-articles/understanding-rl-circuit-operation-and-time-constant/.
41. *Time Constant Formula* https://www.keysight.com/used/be/en/knowledge/formulas/time-constant-formula.

A

Source Code

```
"""
PWM Generator: generates two complementary PWM waves with a peak to peak voltage of 3.3V. The frequency and the duty cycle can be changed on a webserver by filling in the IP address given in the serial monitor in a web browser. To work, the ESP32 S3 board must connect to the same WiFi or Hotspot network. The frequency range is set from 1kHZ to 100kHz and the dutycycle range is 20% to 80%. This may be easily adjusted in the code.
"""

#include <WiFi.h>
#include <WebServer.h>
#include "driver/mcpwm.h"

// PWM Configuration
#define GPIO_PWM0A_OUT 4   // UNIT0 TIMER0 A
#define GPIO_PWM0B_OUT 5   // UNIT0 TIMER0 B
#define GPIO_PWM1A_OUT 17  // UNIT0 TIMER1 A
#define GPIO_PWM1B_OUT 16  // UNIT0 TIMER1 B

// Default values
int freq0 = 20000;        // 20kHz default frequency
float duty0 = 50.0;       // 50% default duty cycle
const int MAX_FREQ = 100000; // 100kHz maximum frequency

// WiFi credentials
const char* ssid = ".............";
const char* password = ".............";

WebServer server(80);

void setuppwm() {
    // Initialize GPIOs
    mcpwm_gpio_init(MCPWM_UNIT_0, MCPWM0A, GPIO_PWM0A_OUT);
    mcpwm_gpio_init(MCPWM_UNIT_0, MCPWM0B, GPIO_PWM0B_OUT);
    mcpwm_gpio_init(MCPWM_UNIT_0, MCPWM1A, GPIO_PWM1A_OUT);
    mcpwm_gpio_init(MCPWM_UNIT_0, MCPWM1B, GPIO_PWM1B_OUT);

    // Configure PWM0
    mcpwm_config_t pwm_config0 = {
        .frequency = freq0,
        .cmpr_a = duty0,
        .cmpr_b = duty0,
        .duty_mode = MCPWM_DUTY_MODE_0,
        .counter_mode = MCPWM_UP_COUNTER
    };

    // Initialize PWM timer
    mcpwm_init(MCPWM_UNIT_0, MCPWM_TIMER_0, &pwm_config0);

    // Enable complementary PWM (optional)
```

```
    mcpwm_deadtime_enable(MCPWM_UNIT_0, MCPWM_TIMER_0,
    MCPWM_ACTIVE_HIGH_COMPLIMENT_MODE, 10, 10);
}

void updatePWM() {
    mcpwm_config_t pwm_config0 = {
        .frequency = freq0,
        .cmpr_a = duty0,
        .cmpr_b = duty0,
        .duty_mode = MCPWM_DUTY_MODE_0,
        .counter_mode = MCPWM_UP_COUNTER
    };

    mcpwm_init(MCPWM_UNIT_0, MCPWM_TIMER_0, &pwm_config0);
}

void handleRoot() {
    String html = R"=====(
<!DOCTYPE␣HTML>
<html>
<head>
␣␣␣␣<meta␣name="viewport"␣content="width=device-width, initial-scale=1">
␣␣␣␣<style>
␣␣␣␣␣␣␣␣body␣{␣font-family:␣Arial;␣text-align:␣center;␣margin:␣0␣auto;␣padding:␣20px;␣}
␣␣␣␣␣␣␣␣.slider-container␣{␣margin:␣20px␣auto;␣width:␣80%;␣max-width:␣400px;␣}
␣␣␣␣␣␣␣␣.slider␣{␣width:␣100%;␣}
␣␣␣␣␣␣␣␣.value-display␣{␣margin:␣10px;␣font-size:␣18px;␣}
␣␣␣␣␣␣␣␣.input-field␣{␣width:␣100px;␣padding:␣8px;␣font-size:␣16px;␣}
␣␣␣␣␣␣␣␣.btn␣{␣padding:␣10px␣20px;␣font-size:␣16px;␣background-color:␣#4CAF50;␣color:␣white;␣
    border:␣none;␣border-radius:␣4px;␣cursor:␣pointer;␣}
␣␣␣␣␣␣␣␣.btn:hover␣{␣background-color:␣#45a049;␣}
␣␣␣␣</style>
</head>
<body>
␣␣␣␣<h1>ESP32␣PWM␣Control</h1>

␣␣␣␣<div␣class="slider-container">
␣␣␣␣␣␣␣␣<h2>Frequency␣Control</h2>
␣␣␣␣␣␣␣␣<p>Current␣Frequency:␣<span␣id="freqValue">)=====";
    html += String(freq0);
    html += R"=====(</span>␣Hz</p>
␣␣␣␣␣␣␣␣<input␣type="range"␣min="1000"␣max="100000"␣value=")=====";
␣␣␣␣html␣+=␣String(freq0);
␣␣␣␣html␣+=␣R"=====("␣class="slider"␣id="freqSlider">
␣␣␣␣␣␣␣␣<p>Or␣enter␣value␣(1kHz-100kHz):</p>
␣␣␣␣␣␣␣␣<input␣type="number"␣id="freqInput"␣class="input-field"␣min="1000"␣max="100000"␣value
    =")=====";
␣␣␣␣html␣+=␣String(freq0);
␣␣␣␣html␣+=␣R"=====(">
␣␣␣␣␣␣␣␣<button␣onclick="updateFrequency()"␣class="btn">Set␣Frequency</button>
␣␣␣␣</div>

␣␣␣␣<div␣class="slider-container">
␣␣␣␣␣␣␣␣<h2>Duty␣Cycle␣Control</h2>
␣␣␣␣␣␣␣␣<p>Current␣Duty␣Cycle:␣<span␣id="dutyValue">)=====";
    html += String(duty0);
    html += R"=====(</span>␣%</p>
␣␣␣␣␣␣␣␣<input␣type="range"␣min="20"␣max="80"␣value=")=====";
␣␣␣␣html␣+=␣String(duty0);
␣␣␣␣html␣+=␣R"=====("␣class="slider"␣id="dutySlider">
␣␣␣␣␣␣␣␣<p>Or␣enter␣value␣(20%-80%):</p>
␣␣␣␣␣␣␣␣<input␣type="number"␣id="dutyInput"␣class="input-field"␣min="20"␣max="80"␣value=")
    =====";
␣␣␣␣html␣+=␣String(duty0);
␣␣␣␣html␣+=␣R"=====(">
␣␣␣␣␣␣␣␣<button␣onclick="updateDuty()"␣class="btn">Set␣Duty␣Cycle</button>
␣␣␣␣</div>

␣␣␣␣<script>
␣␣␣␣␣␣␣␣//␣Update␣slider␣position␣when␣input␣field␣changes
␣␣␣␣␣␣␣␣document.getElementById('freqInput').addEventListener('input',␣function()␣{
```

```
␣␣␣␣␣␣␣␣␣␣␣␣document.getElementById('freqSlider').value␣=␣this.value;
␣␣␣␣␣␣␣␣␣␣});
␣␣␣␣␣␣␣␣␣␣document.getElementById('dutyInput').addEventListener('input',␣function()␣{
␣␣␣␣␣␣␣␣␣␣␣␣document.getElementById('dutySlider').value␣=␣this.value;
␣␣␣␣␣␣␣␣␣␣});
␣␣␣␣␣␣␣␣␣␣//␣Update␣input␣field␣when␣slider␣changes
␣␣␣␣␣␣␣␣␣␣document.getElementById('freqSlider').addEventListener('input',␣function()␣{
␣␣␣␣␣␣␣␣␣␣␣␣document.getElementById('freqValue').textContent␣=␣this.value;
␣␣␣␣␣␣␣␣␣␣␣␣document.getElementById('freqInput').value␣=␣this.value;
␣␣␣␣␣␣␣␣␣␣});
␣␣␣␣␣␣␣␣␣␣document.getElementById('dutySlider').addEventListener('input',␣function()␣{
␣␣␣␣␣␣␣␣␣␣␣␣document.getElementById('dutyValue').textContent␣=␣this.value;
␣␣␣␣␣␣␣␣␣␣␣␣document.getElementById('dutyInput').value␣=␣this.value;
␣␣␣␣␣␣␣␣␣␣});
␣␣␣␣␣␣␣␣␣␣function␣updateFrequency()␣{
␣␣␣␣␣␣␣␣␣␣␣␣var␣freq␣=␣document.getElementById('freqInput').value;
␣␣␣␣␣␣␣␣␣␣␣␣if(freq␣<␣1000)␣freq␣=␣1000;
␣␣␣␣␣␣␣␣␣␣␣␣if(freq␣>␣100000)␣freq␣=␣100000;
␣␣␣␣␣␣␣␣␣␣␣␣var␣xhr␣=␣new␣XMLHttpRequest();
␣␣␣␣␣␣␣␣␣␣␣␣xhr.open("GET",␣"/setFreq?value="␣+␣freq,␣true);
␣␣␣␣␣␣␣␣␣␣␣␣xhr.send();
␣␣␣␣␣␣␣␣␣␣␣␣document.getElementById('freqValue').textContent␣=␣freq;
␣␣␣␣␣␣␣␣␣␣␣␣document.getElementById('freqSlider').value␣=␣freq;
␣␣␣␣␣␣␣␣␣␣}
␣␣␣␣␣␣␣␣␣␣function␣updateDuty()␣{
␣␣␣␣␣␣␣␣␣␣␣␣var␣duty␣=␣document.getElementById('dutyInput').value;
␣␣␣␣␣␣␣␣␣␣␣␣if(duty␣<␣20)␣duty␣=␣20;
␣␣␣␣␣␣␣␣␣␣␣␣if(duty␣>␣80)␣duty␣=␣80;
␣␣␣␣␣␣␣␣␣␣␣␣var␣xhr␣=␣new␣XMLHttpRequest();
␣␣␣␣␣␣␣␣␣␣␣␣xhr.open("GET",␣"/setDuty?value="␣+␣duty,␣true);
␣␣␣␣␣␣␣␣␣␣␣␣xhr.send();
␣␣␣␣␣␣␣␣␣␣␣␣document.getElementById('dutyValue').textContent␣=␣duty;
␣␣␣␣␣␣␣␣␣␣␣␣document.getElementById('dutySlider').value␣=␣duty;
␣␣␣␣␣␣␣␣␣␣}
␣␣␣␣␣␣␣␣</script>
</body>
</html>
)=====";

    server.send(200, "text/html", html);
}

void handleSetFreq() {
    if (server.hasArg("value")) {
        freq0 = server.arg("value").toInt();
        if (freq0 < 1000) freq0 = 1000;
        if (freq0 > MAX_FREQ) freq0 = MAX_FREQ;

        updatePWM();
        server.send(200, "text/plain", "Frequency␣set␣to␣" + String(freq0) + "␣Hz");
    } else {
        server.send(400, "text/plain", "Missing␣value␣parameter");
    }
}

void handleSetDuty() {
    if (server.hasArg("value")) {
        duty0 = server.arg("value").toFloat();
        if (duty0 < 20) duty0 = 20;
        if (duty0 > 80) duty0 = 80;

        updatePWM();
```

```
        server.send(200, "text/plain", "Duty cycle set to " + String(duty0) + "%");
    } else {
        server.send(400, "text/plain", "Missing value parameter");
    }
}

void setup() {
    Serial.begin(115200);

    // Connect to WiFi
    WiFi.begin(ssid, password);
    Serial.println("Connecting to WiFi...");
    while (WiFi.status() != WL_CONNECTED) {
        delay(500);
        Serial.print(".");
    }
    Serial.println("");
    Serial.println("WiFi connected");
    Serial.println("IP address: ");
    Serial.println(WiFi.localIP());

    // Initialize PWM
    setuppwm();

    // Set up web server
    server.on("/", handleRoot);
    server.on("/setFreq", handleSetFreq);
    server.on("/setDuty", handleSetDuty);
    server.begin();
    Serial.println("HTTP server started");
}

void loop() {
    server.handleClient();
}
```

```
"""
Plot generator: input is a list of .csv file paths and the output is a plot with the
    different graphs. An arbitrary amount of file paths can be inserted into the list.
"""

import pandas as pd
import matplotlib.pyplot as plt
import os

def read_oscilloscope_csv(file_path):
    """Read oscilloscope CSV file and return time and voltage data"""
    # Read the CSV file, skipping metadata rows and handling the format
    df = pd.read_csv(file_path, skiprows=14, header=None, usecols=[3, 4],
                     names=['time', 'voltage'], dtype=float)
    return df['time'], df['voltage']

def plot_oscilloscope_data(file_paths):
    """Plot multiple oscilloscope CSV files on the same graph"""
    plt.figure(figsize=(12, 6))

    for file_path in file_paths:
        try:
            time, voltage = read_oscilloscope_csv(file_path)
            # Extract filename without extension for legend
            filename = os.path.splitext(os.path.basename(file_path))[0]
            plt.plot(time, voltage, label=filename, alpha=0.5)
        except Exception as e:
            print(f"Error processing {file_path}: {str(e)}")

    plt.xlabel('Time (s)')
    plt.ylabel('Voltage (V)')
    plt.title('Oscilloscope Measurements')
    plt.grid(True)
    plt.legend()
    plt.tight_layout()
```

```
    plt.show()

if __name__ == "__main__":
    # Example usage - replace with your actual file paths
    file_paths = [
        "file_path1",  # Replace with your file paths
        "file_path2",
        "file_path3"
    ]

    plot_oscilloscope_data(file_paths)
```

B

Additional resources

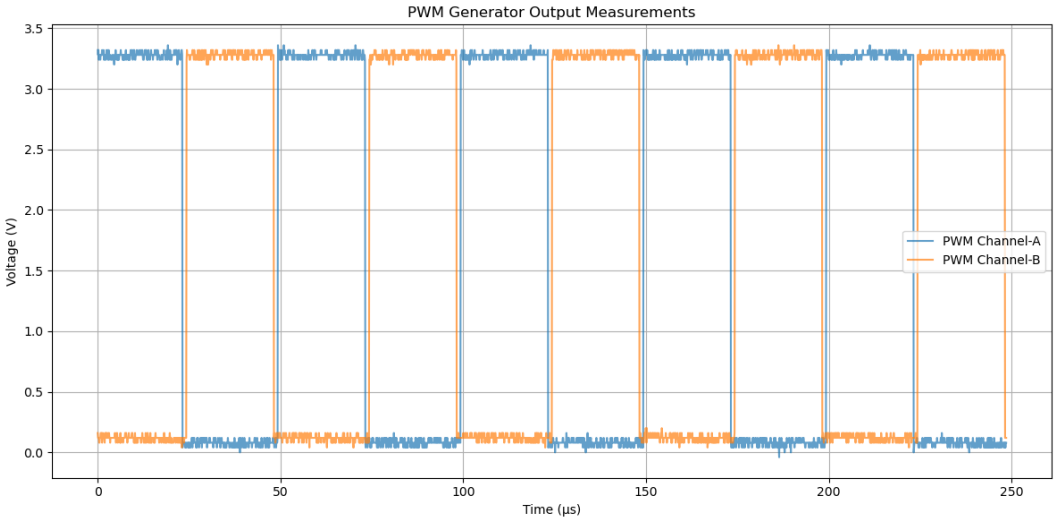

Figure B.1: Complementary PWM generator output measurements

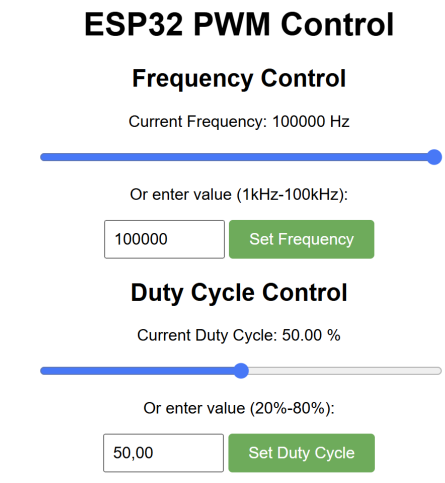

Figure B.2: Screenshot of PWM generator web server

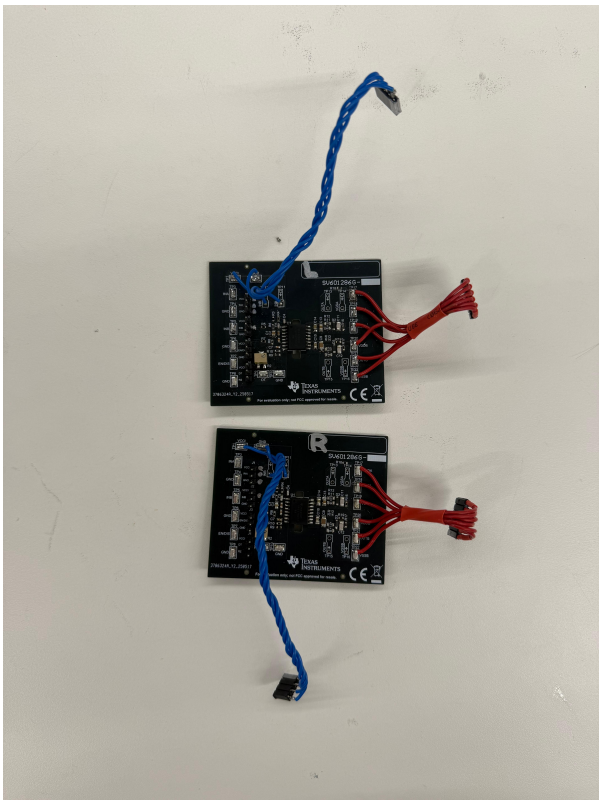

Figure B.3: Gate driver boards for the bipolar driver [24]

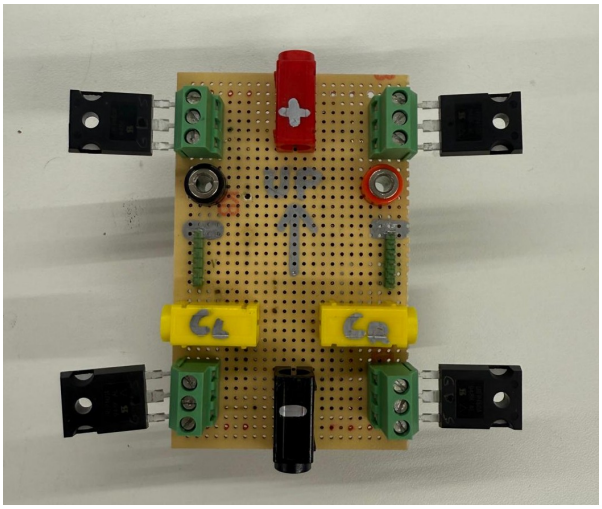

Figure B.4: IRFP460A based H-bridge for the bipolar driver

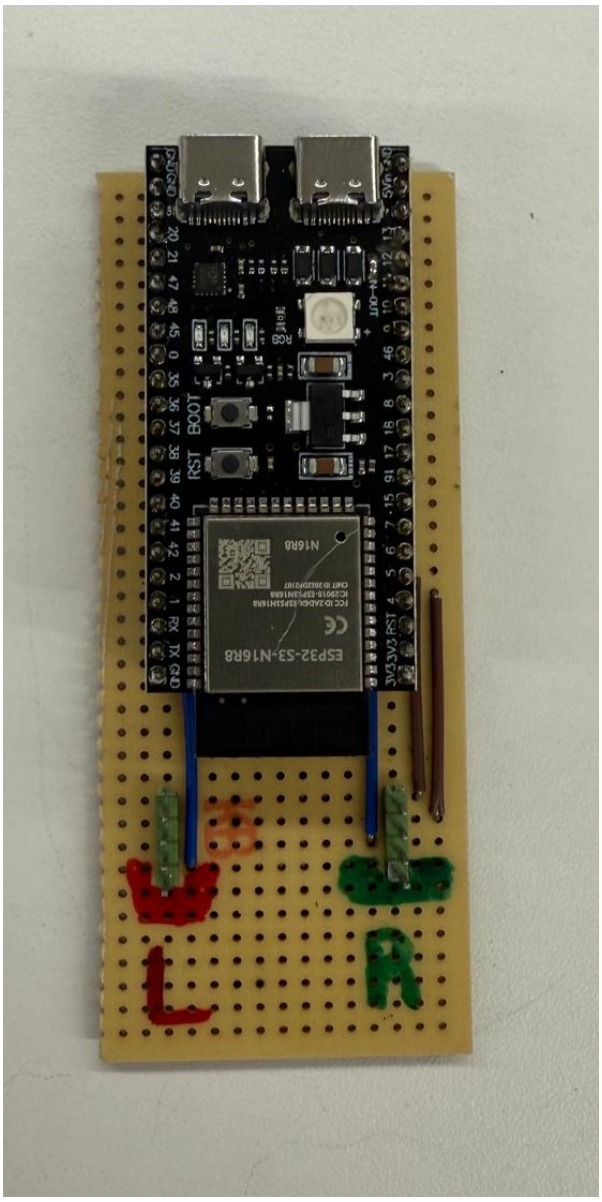

Figure B.5: ESP32-S3 based PWM generator

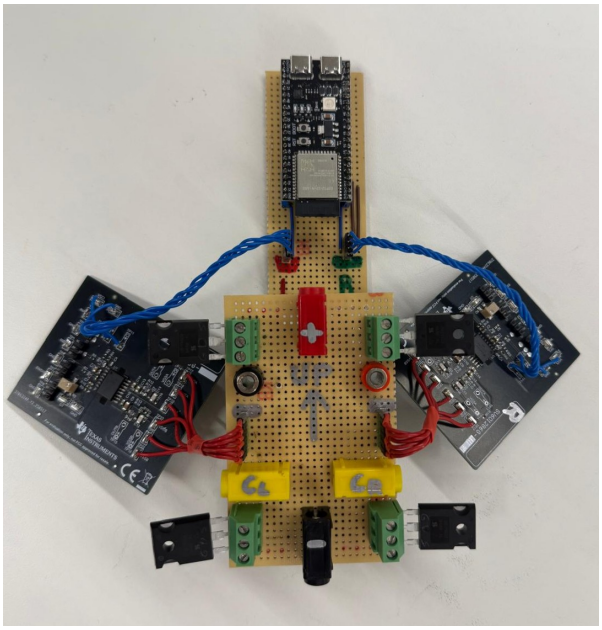

Figure B.6: Complete bipolar driver circuit

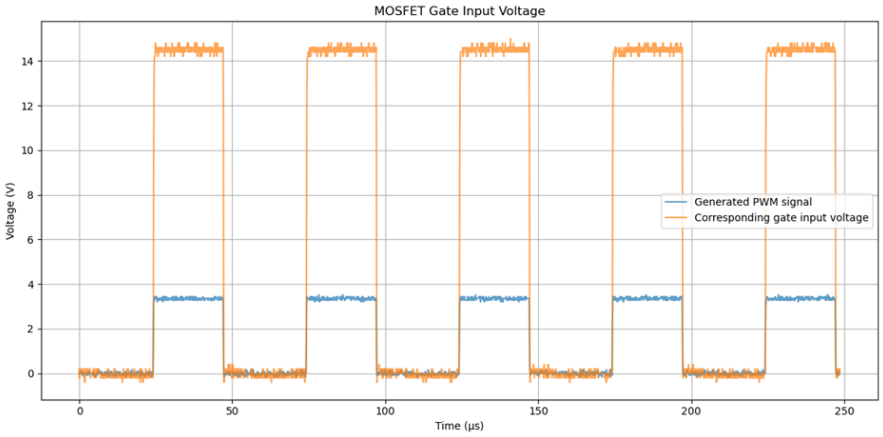

Figure B.7: Amplified gate signal by half bridge driver module

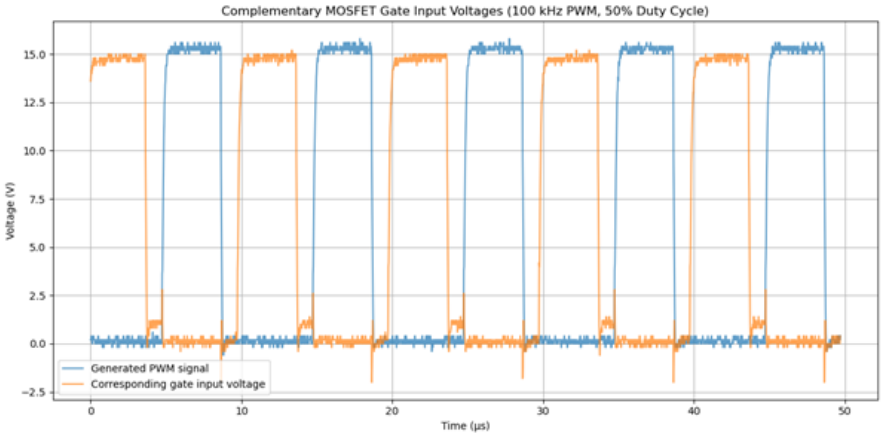

Figure B.8: Complementary gate signals at 100kHz

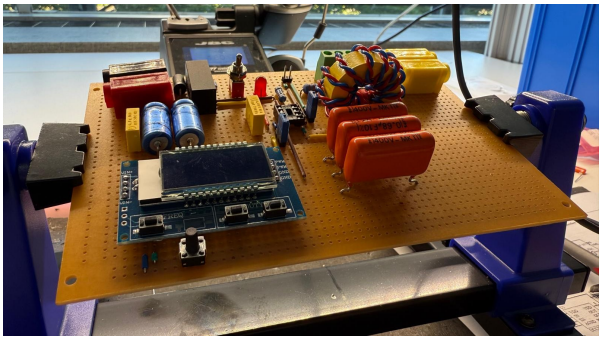

Figure B.9: Built Unipolar driver with intergated PWM Generator with display

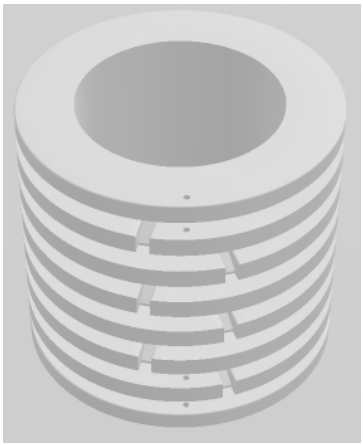

Figure B.10: Secondary spool with 7 isolated compartments

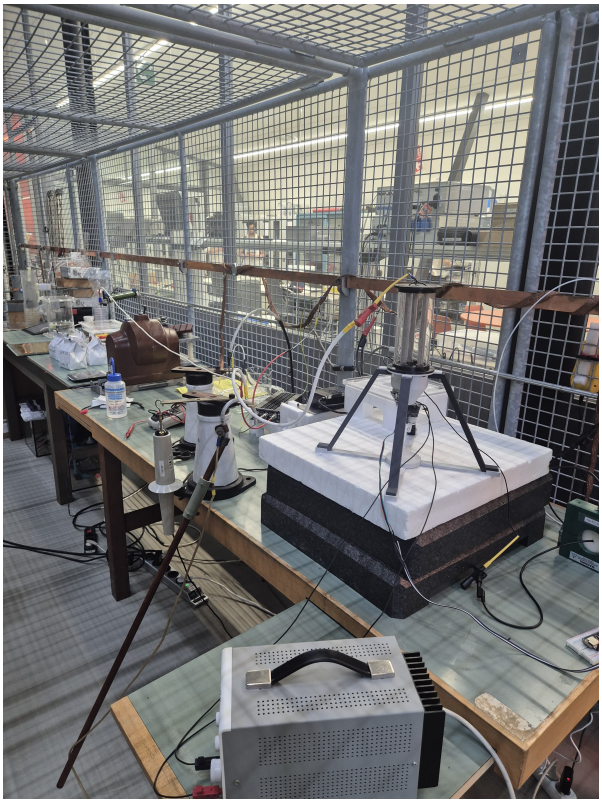

Figure B.11: Triple coaxial load testing setup

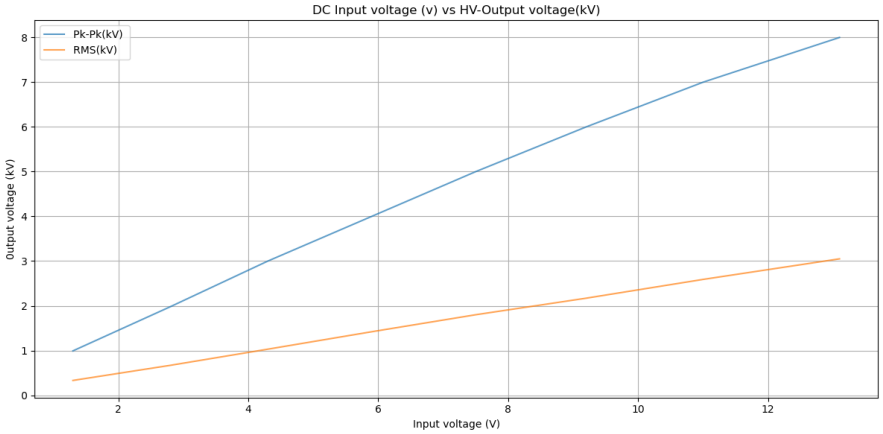

Figure B.12: Linear relation between the driver input voltage and the HV output

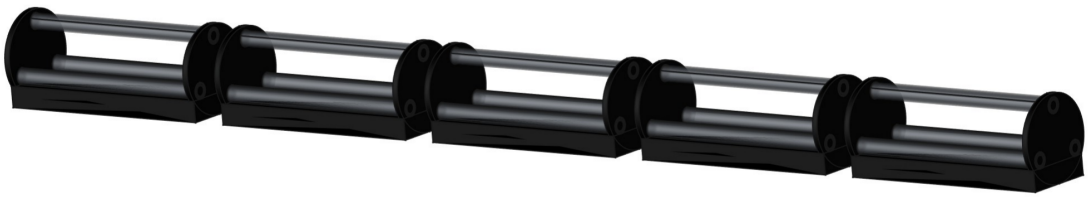

Figure B.13: Segmented setup

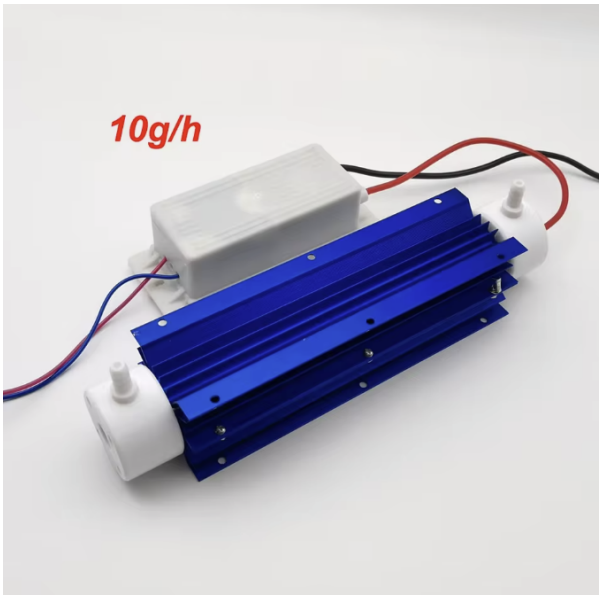

Figure B.14: Commercial Ozone generator with high voltage AC power supply

C

Transformer designs

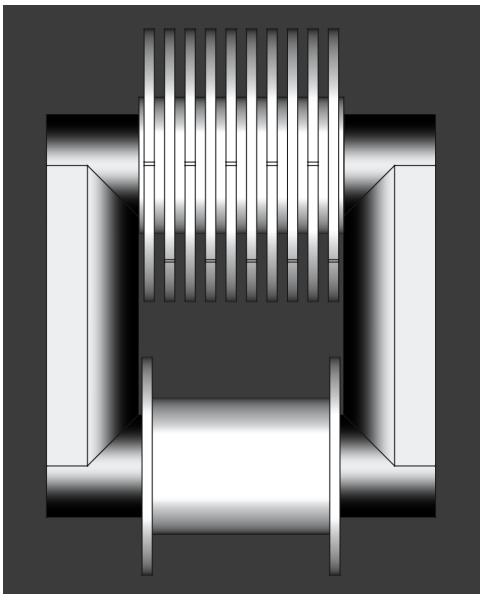

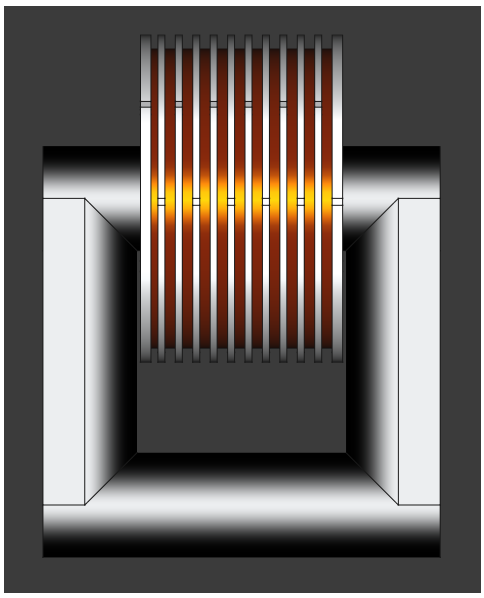

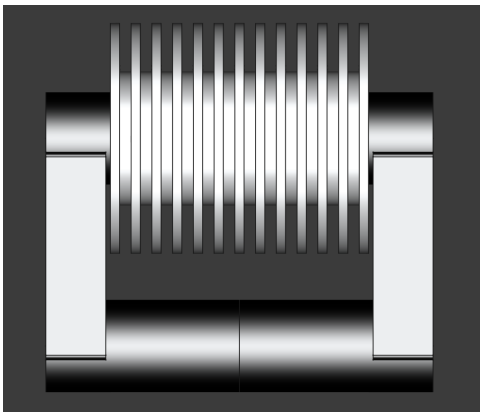

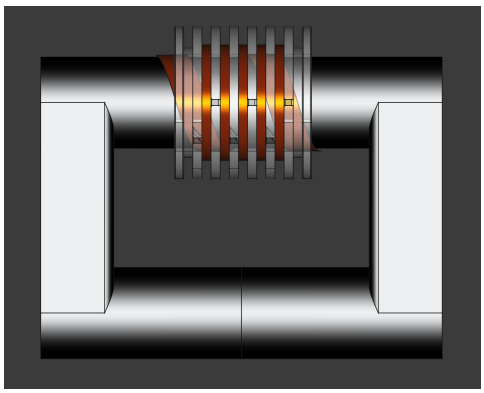

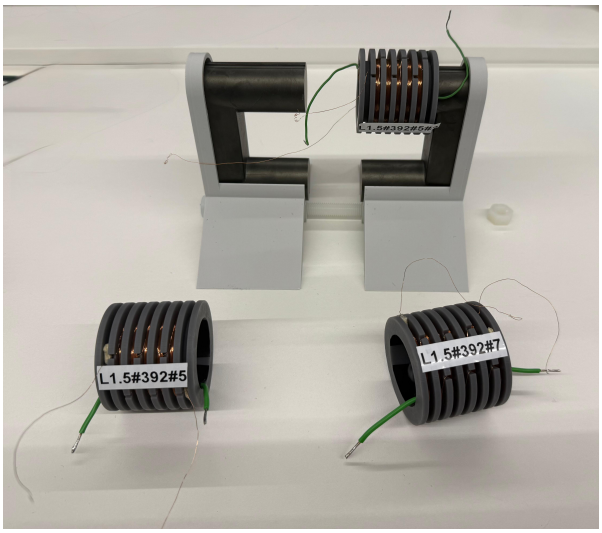

Figure C.1: Transformer mount with coils

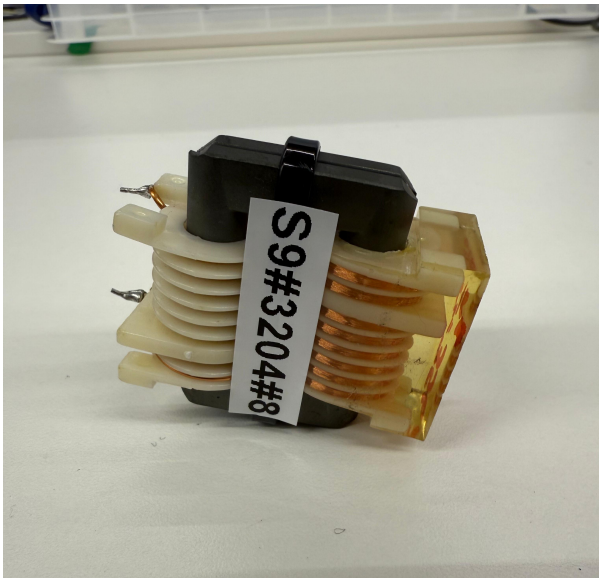

Figure C.2: Small high voltage transformer (UY10;3204;8)

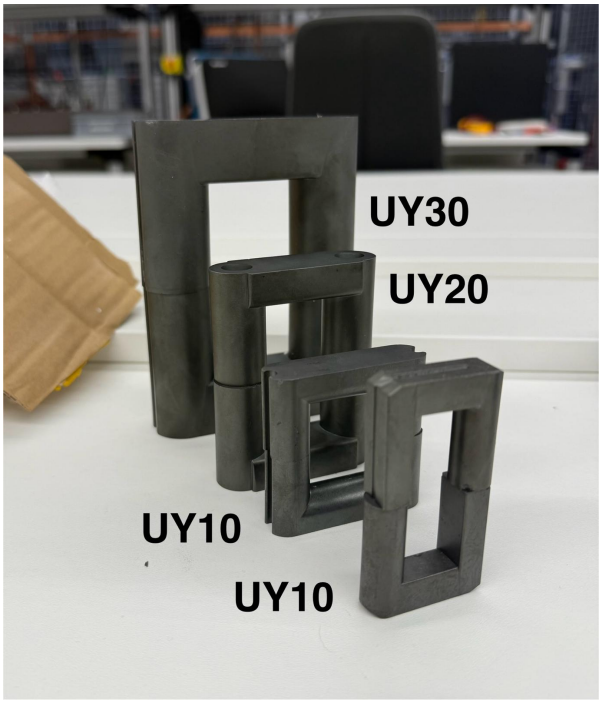

Figure C.3: Ferrite core sizes